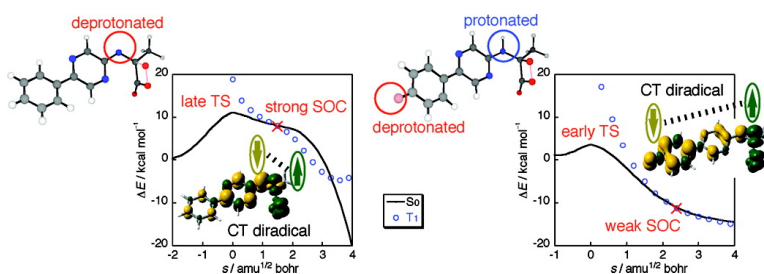Article

Regulation Mechanism of Spin–Orbit Coupling in Charge-Transfer-Induced Luminescence of Imidazopyrazinone Derivatives

Hiroshi Isobe, Syusuke Yamanaka, Seiki Kuramitsu, and Kizashi Yamaguchi

More About This Article

Additional resources and features associated with this article are available within the HTML version:

- Supporting Information
- Links to the 2 articles that cite this article, as of the time of this article download
- Access to high resolution figures
- Links to articles and content related to this article
- Copyright permission to reproduce figures and/or text from this article

View the Full Text HTML

Regulation Mechanism of Spin−Orbit Coupling in Charge-Transfer-Induced Luminescence of Imidazopyrazinone Derivatives

Hiroshi Isobe,*,† Syusuke Yamanaka,† Seiki Kuramitsu,‡ and Kizashi Yamaguchi†

Department of Chemistry and Department of Biological Sciences, Graduate School of Science, Osaka University, Toyonaka, Osaka 560-0043, Japan

Received May 28, 2007; E-mail: isobe@chem.sci.osaka-u.ac.jp

Abstract: The spin transition in the reactions of the derivatives of imidazo[1,2-*a*]pyrazin-3(7*H*)-one (**1H**) with a triplet molecular oxygen ($^3O_2$) has been investigated by the geometry optimization at the B3LYP/6-31+G(d) level and the evaluation of the electronic matrix elements for spin−orbit coupling (SOC) using the full Pauli−Breit SOC operator. The reductive activation for the $^3O_2$ reaction is affected by the proton activity and solvent polarity of a surrounding reaction field. In a polar aprotic solvent, a base-prompted anionic substrate may react with $^3O_2$ in a stepwise manner through complete electron transfer from the substrate anion to $^3O_2$, while the irreversible concerted $^3O_2$ addition via intersystem crossing may become complete in a less polar solvent. SOC in the thermal decomposition of a resulting peroxide adduct can be controlled by the protonation state of the substrate. There exists an optimal protonation state for the suppression of SOC in the charge-transfer-induced luminescence (CTIL) of the peroxide, which is closely related with the ability of a substituent to donate an electron. This will constitute a necessary condition for the high efficiency of chemi- and bioluminescence.

1. Introduction

Chemiluminescence and bioluminescence phenomena have recently received a considerable amount of attention not only as a subject of academic interest[1,2] but also as a useful analytical tool in the forefront of life sciences and in medical and pharmaceutical applications.[3] There is continuing research on the efficient enzymatic catalysis that can convert chemical energy into photon energy with a high yield. At the same time, there is also an increasing need for theoretical models, which reveal fundamental factors that control the catalytic activity. In this context, we have investigated the chemiluminescence mechanism with quantum chemical calculations[4] and have suggested the importance of charge-transfer-induced luminescence (CTIL) with polarization-induced branching excitation processes.[4a]

A biological system uses a triplet molecular oxygen ($^3O_2$) as an oxidant to extract sufficiently high exothermicity from the oxidation of a substrate called luciferin under catalysis by an enzyme called luciferase to allow the emission of a photon of visible light, as shown in eq 1, in which Lu denotes a luciferin, Pox, a peroxide or a hydroperoxide adduct, and P, an oxyluciferin.[2]

$$Lu + {}^3O_2 \rightarrow {}^{1,3}Pox \rightarrow {}^1P* \rightarrow {}^1P + h\nu \qquad (1)$$
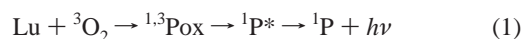
The final product of oxidation is formed in a singlet excited state; therefore, the spin-multiplicity change is required somewhere during the course of the reaction. The mechanism for overcoming the spin prohibition for the $^3O_2$ reaction in a controlled manner is a subject of some discussion and controversy in chemi- and bioluminescence and other oxygenation reactions. A large amount of work has been directed toward the oxygen activation by enzymes, and the importance of the stepwise pathway via electron and proton transfers and the spin catalysis by a paramagnetic metal ion has been suggested.[5−7]

In addition to the activation of $^3O_2$, there is one further important issue associated with spin transition in chemi- and bioluminescence that we must not ignore. That is the intersystem crossing induced by spin−orbit coupling (SOC) in the thermal

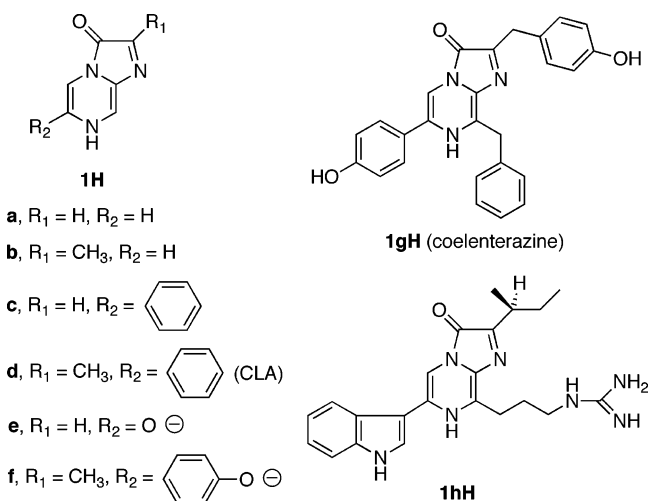† Department of Chemistry.

‡ Department of Biological Sciences.

(1) (a) McCapra, F. *Q. Rev. Chem. Soc.* **1966**, *20*, 485. (b) Wilson, T. *Int. Rev. Sci., Phys. Chem. Ser. 2* **1976**, *9*, 265. (c) Adam, W. *Pure Appl. Chem.* **1980**, *52*, 2591. (d) Schuster, G. B. *Acc. Chem. Res.* **1979**, *12*, 366. (e) Matsumoto, M. *J. Photochem. Photobiol., C* **2004**, *5*, 27.

(2) (a) Goto, T.; Kishi, Y. *Angew. Chem., Int. Ed. Engl.* **1968**, *7*, 407. (c) McCapra, F. *Acc. Chem. Res.* **1976**, *9*, 201. (c) Hastings, J. W. *J. Mol. Evol.* **1983**, *19*, 309.

(3) (a) Beck, S.; Köster, H. *Anal. Chem.* **1990**, *62*, 2258. (b) Mayer, A.; Neuenhofer, S. *Angew. Chem., Int. Ed. Engl.* **1994**, *33*, 1044. (c) Adam, W.; Reinhardt, D.; Saha-Möller, C. R. *Analyst* **1996**, *121*, 1527. (d) Roda, A.; Guardigli, M.; Michelini, E.; Mirasoli, M.; Pasini, P. *Anal. Chem.* **2003**, *75*, 462A.

(4) (a) Isobe, H.; Takano, Y.; Okumura, M.; Kuramitsu, S.; Yamaguchi, K. *J. Am. Chem. Soc.*, **2005**, *127*, 8667. (b) Takano, Y.; Tsunesada, T.; Isobe, H.; Yoshioka, Y.; Yamaguchi, K.; Saito, I. *Bull. Chem. Soc. Jpn.* **1999**, *72*, 213. (c) Yoshioka, Y.; Yamanaka, S.; Yamada, S.; Kawakami, T.; Nishino, M.; Yamaguchi, K.; Nishinaga, A. *Bull. Chem. Soc. Jpn.* **1996**, *69*, 2701. (d) Yamaguchi, K. In *Singlet Oxygen*; Frimer, A. A., Ed.; CRC Press: Boca Raton, FL, 1985; Vol. III, p 119.

(5) Sawyer, D. T. In *Oxygen complexes and oxygen activation by transition metals*; Martell, A. E., Sawyer, D. T., Eds.; Plenum Press, New York, 1988; p 131.

(6) (a) Klinman, J. P. *J. Biol. Inorg. Chem.* **2001**, *6*, 1. (b) Klinman, J. P. *Acc. Chem. Res.* **2007**, *40*, 325.

(7) (a) Prabhakar, R.; Siegbahn, P. E. M.; Minaev, B. F.; Ågren, H. *J. Phys. Chem. B* **2002**, *106*, 3742. (b) Prabhakar, R.; Siegbahn, P. E. M.; Minaev, B. F.; Ågren, H. *J. Phys. Chem. B* **2004**, *108*, 13882.

Chart 1

1H

a, $R_1 = H$, $R_2 = H$

b, $R_1 = CH_3$, $R_2 = H$

c, $R_1 = H$, $R_2 = $ ⬡

d, $R_1 = CH_3$, $R_2 = $ ⬡ (CLA)

e, $R_1 = H$, $R_2 = $ O⊖

f, $R_1 = CH_3$, $R_2 = $ ⬡—O⊖

1gH (coelenterazine)

1hH

decomposition of a peroxide adduct, which is responsible for deactivation when the dissociating peroxide crosses from a singlet to a triplet state and decays in the corresponding triplet state. The transition back from the triplet to a singlet excited state cannot occur, since the triplet state is usually lower in energy. The spin-multiplicity distribution and the excitation yield in product formation are, therefore, inherently dependent on the SOC in the crossing seam between the singlet and triplet states. The luciferase should control a specific excitation pathway that suppresses SOC sufficiently such that the chemical energy of a peroxide is held most effectively in the singlet excited state of an emitter responsible for fluorescence, while phosphorescence is often observed in chemiluminescence as a result of facile spin-symmetry-forbidden nonradiative transition from the singlet to the triplet state.[1] Although strong SOC in the homolytic diradical state of a dissociating peroxide has been a subject of study for a long time,[8] surprisingly few attempts have so far been made at understanding the regulation mechanism of SOC in the charge-transfer diradical state. The extent of energy leak to a nonluminescent triplet state is quite difficult to detect by experiment, and therefore, there is limited information available on the violation of spin-symmetry conservation along the reaction pathway. The details need to be analyzed theoretically. This has prompted us to evaluate numerically the electronic matrix elements for SOC in the thermolysis of peroxides, a subject that has not appeared in the literature.

In a present article, we report a hybrid density functional theory (B3LYP) study of the reactions of the derivatives of imidazo[1,2-*a*]pyrazin-3(7*H*)-one (**1H**), as shown in Chart 1, with a molecular oxygen. The imidazopyrazinone skeleton is a core structure of luciferins, **1gH** (coelenterazine) and **1hH**, which are isolated from marine bioluminescent organisms, the jellyfish *Aequorea*[9] and the crustacean *Cypridina* (*Vargula*).[10] A *Cypridina* luciferin analogue (CLA, **1dH**) and its derivatives[10−14] have often been used as a chemiluminescence probe for the

detection and/or measurement of reactive oxygen species because of their high reactivity toward superoxide anion and singlet oxygen at physiological temperature and pH.[14] The main purpose of this article is to elucidate the influence of the protonation state of imidazopyrazinone substrates on their reactivity toward $^3O_2$ and on the chemistry of resulting peroxide adducts. The phenomenon of spin transition is specifically emphasized to understand the substrate activation for the $^3O_2$ reaction and the regulation mechanism of SOC in the thermolysis of peroxides. We feel that the oxygenations of imidazopyrazinones provide good information on the subjects. Other important issues associated with regioselectivity, substituent effects, thermolysis of luciferins, and the roles of surrounding amino acid residues will be reported elsewhere.

2. Theoretical Background and Computational Details

The geometries of reactants, transition structures (TS), intermediates, and products reported in this study were obtained by the full optimization at the B3LYP/6-31+G(d)[15,16] level, and the harmonic frequency analysis was carried out to characterize the stationary points and to derive zero-point vibrational corrections (ZPC) and thermodynamics effects at 298 K by statistical mechanics calculations. The open-shell systems were treated by unrestricted (U) B3LYP (UB3LYP). The serious difficulty in studying singlet diradical species using the broken-symmetry approach arises from the fact that the spin-unrestricted wave functions exhibit a large contamination from higher spin states. To estimate singlet UB3LYP energies with annihilation of the spin contamination, we applied our approximate spin projection (AP) scheme,[17] as described in eqs 2 and 3, in which ^XE is the total energy and $^X\langle S^2 \rangle$ is the total angular momentum of the spin state X.

$$^{singlet}E_{AP} = {}^{singlet}E + c_{SC}[^{singlet}E - {}^{triplet}E] \qquad (2)$$

$$c_{SC} = \frac{{}^{singlet}\langle S^2 \rangle}{{}^{triplet}\langle S^2 \rangle - {}^{singlet}\langle S^2 \rangle} \qquad (3)$$

(8) (a) Turro, N. J.; Devaquet, A. *J. Am. Chem. Soc.* **1975**, *97*, 3859. (b) Wilsey, S.; Bernardi, F.; Olivucci, M.; Robb, M. A.; Murphy, S.; Adam, W. *J. Phys. Chem. A* **1999**, *103*, 1669. (c) Tanaka, C.; Tanaka, J. *J. Phys. Chem. A* **2000**, *104*, 2078.

(9) (a) Shimomura, O.; Johnson, F. H.; Saiga, Y. *J. Cell. Comp. Physiol.* **1962**, *59*, 223. (b) Shimomura, O.; Johnson, F. H.; Saiga, Y. *Science* **1963**, *140*, 1339. (c) Johnson, F. H.; Shimomura, O. *Methods Enzymol.* **1978**, *57*, 271. (d) Ohmiya, Y.; Hirano, T. *Chem. Biol.* **1996**, *3*, 337. (e) Vysotski, E. S.; Lee, J. *Acc. Chem. Res.* **2004**, *37*, 405.

(10) (a) Goto, T. *Pure. Appl. Chem.* **1968**, *17*, 421. (b) Kishi, Y.; Goto, T.; Hirata, Y.; Shimomura, O.; Johnson, F. H. *Tetrahedron Lett.* **1966**, 3427. (c) Shimomura, O.; Johnson, F. H. *Photochem. Photobiol.* **1970**, *12*, 291. (d) Shimomura, O.; Johnson, F. H. *Biochem. Biophys. Res. Commun.* **1971**, *44*, 340. (e) Nakamura, H.; Aizawa, M.; Takeuchi, D.; Murai, A.; Shimomura, O. *Tetrahedron Lett.* **2000**, *41*, 2185.

(11) (a) McCapra, F.; Chang, Y. O. *J. Chem. Soc., Chem. Commun.* **1967**, 1011. (b) McCapra, F.; Chang, Y. O.; Francois, V. P. *J. Chem. Soc., Chem. Commun.* **1968**, 22.

(12) (a) Fujimori, K.; Nakajima, H.; Akutsu, K.; Mitani, M.; Sawada, H.; Nakayama, M. *J. Chem. Soc., Perkin Trans. 2* **1993**, 2405. (b) Akutsu, K.; Nakajima, H.; Katoh, T.; Kino, S.; Fujimori, K. *J. Chem. Soc., Perkin Trans. 2* **1995**, 1699. (c) Fujimori, K.; Komiyama, T.; Tabata, H.; Nojima, T.; Ishiguro, K.; Sawaki, Y.; Tatsuzawa, H.; Nakano, M. *Photochem. Photobiol.* **1998**, *68*, 143.

(13) (a) Kondo, H.; Igarashi, T.; Maki, S.; Niwa, H.; Ikeda, H.; Hirano, T. *Tetrahedron Lett.* **2005**, *46*, 7701. (b) Mori, K.; Maki, S.; Niwa, H.; Ikeda, H.; Hirano, T. *Tetrahedron* **2006**, *62*, 6272. (c) Takahashi, Y.; Kondo, H.; Maki, S.; Niwa, H.; Ikeda, H.; Hirano, T. *Tetrahedron Lett.* **2006**, *47*, 6057.

(14) (a) Goto, T.; Takagi, T. *Bull. Chem. Soc. Jpn.* **1980**, *53*, 822. (b) Sugioka, K.; Nakano, M.; Karashige, S.; Akutagawa, Y.; Goto, T. *FEBS Lett.* **1986**, *197*, 27. (c) Oosthuizen, M. M.; Engelbrecht, M. E.; Lambrechts, H.; Greyling, D.; Levy, R. D. *J. Biolumin. Chemilumin.* **1997**, *12*, 227. (d) Nakano, M. *Cell. Mol. Neurobiol.* **1998**, *18*, 565. (e) Shimomura, O.; Wu, C.; Murai, A.; Nakamura, H. *Anal. Biochem.* **1998**, *258*, 230. (f) Teranishi, K.; Nishiguchi, T. *Anal. Biochem.* **2004**, *325*, 185.

(15) (a) Becke, A. D. *Phys. Rev. A* **1988**, *38*, 3098. (b) Lee, C.; Yang, W.; Parr, R. G. *Phys. Rev. B* **1988**, *37*, 785. (c) Becke, A. D. *J. Chem. Phys.* **1993**, *98*, 5648.

(16) (a) Hariharan, P. C.; Pople, J. A. *Theor. Chim. Acta.* **1973**, *28*, 213. (b) Clark, T.; Chandrasekhar, J.; Spitznagel, G. W.; Schleyer, P. v. R. *J. Comput. Chem.* **1983**, *4*, 294. (c) Frisch, M. J.; Pople, J. A.; Binkley, J. S. *J. Chem. Phys.* **1984**, *80*, 3265.

(17) (a) Yamaguchi, K.; Takahara, Y.; Fueno, T. In *Applied Quantum Chemistry*; Smith, V. H., Ed.; Reidel: Dordrecht, 1986; p. 155. (b) Yamaguchi, K.; Takahara, Y.; Fueno, T.; Houk, K. N. *Theor. Chem. Acta* **1988**, *73*, 337. (c) Takahara, Y.; Yamaguchi, K.; Fueno, T. *Chem. Phys. Lett.* **1989**, *157*, 211; *158*, 95.

The reaction coordinates from the transition structures were determined by the intrinsic-reaction-coordinate (IRC) calculation.[18] All gas-phase calculations were performed with the Gaussian 98 program.[19a]

The solvation of reactants, transition structures, intermediates, and products by the bulk solvent was evaluated by the conductor-like polarizable continuum model (CPCM)[20,21] at the B3LYP/6-31+G(d) level with the cavity built by the united atom Kohn−Sham topological model (UAKS) implemented in Gaussian 03.[19b] The dielectric constants (ϵ) 36.64 and 2.247 were used to represent acetonitrile and benzene solvents. The gas-phase geometries were used for the single-point CPCM calculations of reactants and products, while the geometry optimizations and vibrational frequency calculations were carried out for transition structures and intermediates with solvent corrections at the B3LYP/6-31+G(d) level, since the geometries of singlet species with diradical/zwitterionic character were found to be very sensitive to the solvent polarity. The solvation free energy defined by Ben-Naim (ΔG^*_{solv})[22] was calculated as a sum of free energies arising from electrostatic, cavitation, dispersion/repulsion, and thermal contributions.[23]

We estimated the base strength of reactants, intermediates, and products, here denoted generally by A, in acetonitrile according to the proton-transfer reaction from the conjugate acid (AH$^+$) to pyridine (C$_5$H$_5$N), as expressed in eq 4.

$$AH^+ + C_5H_5N \rightarrow A + C_5H_5NH^+ \qquad \Delta G^*_{sol} \qquad (4)$$
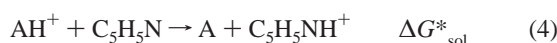
The basicity of a base A is defined as a dissociation constant K_a or its negative logarithm pK_a of the conjugate acid AH$^+$ and can be obtained theoretically as the pK_a shift relative to the experimental value of pyridine (12.53 in acetonitrile),[24] as shown in eqs 5 and 6, in which ΔG^*_{gas} is the gas-phase free-energy change of the proton-transfer reaction (1 mol L^{-1} standard state).

$$pK_a(AH^+) = 12.53 + \frac{\Delta G^*_{sol}}{2.303RT} \qquad (5)$$

$$\Delta G^*_{sol} = \Delta G^*_{gas} + \Delta G^*_{solv}(A) + \Delta G^*_{solv}(C_5H_5NH^+) -$$
$$\Delta G^*_{solv}(AH^+) - \Delta G^*_{solv}(C_5H_5N) \quad (6)$$

If conformational isomers exist, the entropic contribution is considered as a Boltzmann sampling over all possible conformers. The computed basicities are summarized in Figures S1−S3 (Supporting Information).

Standard redox potentials ($E_{red}°$ vs SHE) of reactants in acetonitrile were determined from the half reaction (eq 7), as given in eq 8, in which I_p is the gas-phase adiabatic ionization potential; $-T\Delta S$, the gas-phase entropy term associated with the half reaction; F, the Faraday constant (23.06 kcal mol^{-1} V^{-1}); and ΔSHE, the standard hydrogen electrode potential of -4.43 eV.[25]

(18) (a) Gonzalez, C.; Schlegel, H. B. *J. Chem. Phys* **1989**, *90*, 2154. (b) Gonzalez, C.; Schlegel, H. B. *J. Phys. Chem.* **1990**, *94*, 5523.
(19) (a) Frisch, M. J.; et al. *Gaussian 98*, revision A.11.3; Gaussian, Inc.: Pittsburgh, PA, 2002. (b) Frisch, M. J.; et al. *Gaussian 03*, revision C.02; Gaussian, Inc.: Pittsburgh, PA, 2004.
(20) (a) Klamt, A.; Schüürmann, G. *J. Chem. Soc., Perkin Trans. 2* **1993**, 799. (b) Andzelm, J.; Kölmel, C.; Klamt, A. *J. Chem. Phys.* **1995**, *103*, 9312. (c) Barone, V.; Cossi, M. *J. Phys. Chem. A* **1998**, *102*, 1995. (d) Cossi, M.; Rega, N.; Scalmani, G.; Barone, V. *J. Comput. Chem.* **2003**, *24*, 669.
(21) Takano, Y.; Houk, K. N. *J. Chem. Theory Comput.* **2005**, *1*, 70.
(22) Ben-Naim, A. *J. Phys. Chem.* **1978**, *82*, 792.
(23) Tomasi, J.; Mennucci, B.; Cammi, R. *Chem. Rev.* **2005**, *105*, 2999.
(24) Kaljurand, I.; Kütt, A.; Soovāli, L.; Rodima, T.; Mäemets, V.; Leito, I.; Koppel, I. A. *J. Org. Chem.* **2005**, *70*, 1019.
(25) Reiss, H.; Heller, A. *J. Phys. Chem.* **1985**, *89*, 4207.

$$A(acetonitrile) \rightarrow A^{\bullet+}(acetonitrile) + e^-(gas) \qquad \Delta G^°_{sol} \quad (7)$$

$$E^°_{red}(vs\ SHE) = \Delta G^°_{sol}/F + \Delta SHE$$

$$= I_p(A) + (-T\Delta S + \Delta G^*_{solv}(A^{\bullet+}) - \Delta G^*_{solv}(A))/F + \Delta SHE \quad (8)$$

The computed $E_{red}°$ value of deprotonated CLA, **1d**$^-$, is -0.40 V vs SHE $= -0.67$ V vs SCE; for reference, the experimentally measured anodic peak potential of **1d**$^-$ is reported to be -0.19 V vs SCE in acetonitrile containing 1,1,3,3-tetramethylguanidine (TMG) (0.10 mol L^{-1}).[13a] The computed standard redox potentials of imidazopyrazinone substrates are presented in Table S1.

The spin−orbit coupling (SOC) matrix elements were calculated between triplet and singlet complete-active-space configuration iteration (CASCI) wave functions with respect to the full Pauli−Breit SOC operator ($\hat{H}_{SO}$) that consists of the one-electron ($\hat{H}_{SO1}$) and two-electron ($\hat{H}_{SO2}$) terms, as given in eqs 9−11, in which Z_A is the atomic number of nucleus A; $\hat{s}_i$ and $\hat{l}_{iA}$, the spin and orbital angular momentum operators for an electron i in the framework of the nuclei A; and $\hat{p}_i$, the linear momentum operator.

$$\hat{H}_{SO} = \hat{H}_{SO1} - \hat{H}_{SO2} \qquad (9)$$

$$\hat{H}_{SO1} = \frac{\alpha^2}{2} \sum_i \sum_A \left(\frac{Z_A}{r_{iA}^3}\right) \hat{s}_i \cdot \hat{l}_{iA} \qquad (10)$$

$$\hat{H}_{SO2} = \frac{\alpha^2}{2} \sum_{i \neq j} \left(\frac{1}{r_{ij}^3}\right)(\hat{r}_{ij} \times \hat{p}_i)(\hat{s}_i + 2\hat{s}_j) \qquad (11)$$

$$\left(\frac{\alpha^2}{2} = \frac{e^2h}{4\pi\ m_e^2c^2}\right)$$

The root-mean-squared value of the SOC constant is defined as eq 12.

$$SOC = \left(\sum_{M_S=\pm1,0} \sum_{k=x,y,z} \langle^3\Psi^{(M_S)}|\hat{H}_{SO}|^1\Psi\rangle_k^2\right)^{1/2} \qquad (12)$$

The SOC constant is relevant to the electronic factor of the rate of the intersystem crossing, as determined by the Fermi's Golden Rule.[26] Unless otherwise noted, the SOC matrix elements in eq 12 were evaluated by using the S$_0$/T$_1$ state-averaged complete-active-space self-consistent field (CASSCF) {14,12} (14 electrons in 12 orbitals) wave function with the 6-31+G(d) basis set. The orbitals in the active space were comprised of natural orbitals of broken-symmetry UB3LYP solutions, which are characterized as the mixing of two π orbitals and two π^* orbitals of O$_2$ and eight valence π orbitals of the imidazopyrazinone ring. To reduce the computational demand, the almost doubly occupied and vacant π orbitals of the imidazopyrazinone ring were assigned in the inactive core and virtual orbitals. For the qualitative interpretation of nonzero SOC interaction, we also used Boys localized orbitals[27] generated at the triplet ROHF/6-31+G(d) level as orbitals from which CASCI wave functions are constructed; see text for details. SOC calculations were performed with the GAMESS program package.[28,29]

3. Results and Discussions

3.1. Mechanisms for Oxygenation Reactions of Imidazopyrazinone Derivatives. 3.1.1. Substrate Activation for ^{3}O$_2$ Reaction. We shall begin with the investigation of the reactivity of a triplet molecular oxygen (^{3}O$_2$) toward imidazopyrazinone

(26) (a) Jortner, J. *Pure Appl. Chem.* **1971**, *27*, 389. (b) Lower, S. K.; El-Sayed, M. A. *Chem. Rev.* **1966**, *66*, 199. (c) Avouris, P.; Gelbart, W. M.; El-Sayed, M. A. *Chem. Rev.* **1977**, *77*, 793. (d) Turro, N. J. *Modern Molecular Photochemistry*; University Science Books: Sausalito, CA, 1991.
(27) Foster, J.; Boys, S. F. *Rev. Mod. Phys.* **1960**, *32*, 300.
(28) Schmidt, M. W.; Baldridge, K. K.; Boatz, J. A.; Elbert, S. T.; Gordon, M. S.; Jensen, J. J.; Koseki, S.; Matsunaga, N.; Nguyen, K. A.; Su, S.; Windus, T. L.; Dupuis, M.; Montgomery, J. A. *J. Comput. Chem.* **1993**, *14*, 1347.
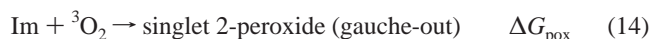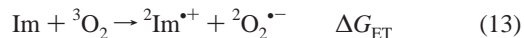(29) Fedorov, D. G.; Gordon, M. S. *J. Chem. Phys.* **2000**, *112*, 5611.

Scheme 1
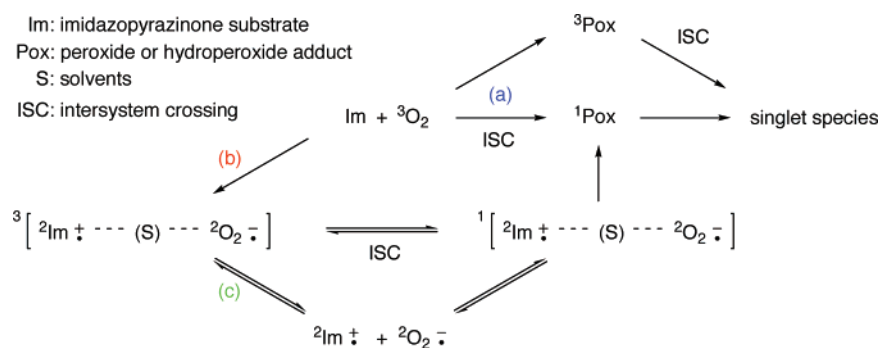
derivatives in a polar homogeneous solution. The thermally activated reactions of $^3O_2$ only allow for single-bond reactions or electron transfer (coupled with proton transfer), leading to the formation of radicals. The most important and controversial aspect of this type oxygenation reaction relates to the question as to whether the complete electron transfer occurs in competition with the direct bonding interaction, since it provides information about the feasibility of the spin transition from the triplet to a singlet state. Scheme 1 outlines possible reaction routes from the triplet reactants to a singlet species, highlighting whether the spin transition occurs before the chemical interaction [via pathway (b) or (c)] or during the chemical interaction [via pathway (a)].

The electron transfer between $^3O_2$ and an imidazopyrazinone substrate (Im) generates a radical pair, $Im^{\bullet+}...O_2^{\bullet-}$, in the overall triplet state. In a polar solvent, the importance of the solvent-separated radical pair, $Im^{\bullet+}...S...O_2^{\bullet-}$, in which solvents (S) have completely penetrated between $Im^{\bullet+}$ and $O_2^{\bullet-}$, has been emphasized.[30] The triplet radical pair must undergo spin transition from the triplet to singlet state to produce a key cyclic dioxetanone functionality via two-bond formation. There are several spin-realignment mechanisms for the radical recombination of the pair.[7,31−34] The weak electronic coupling in the solvent-separated radical pair may result in an exceedingly small energy separation between the singlet and triplet states, so that the hyperfine interaction between the electron spins and nuclear spins may cause the mixing of the triplet and singlet states of the radical pair when the electron exchange interaction is smaller than the hyperfine coupling (ca. 10^{-2} cm^{-1}):[31] $^3[^2Im^{\bullet+}...S...^2O_2^{\bullet-}]$ $\rightleftharpoons$ $^1[^2Im^{\bullet+}...S...^2O_2^{\bullet-}]$. Moreover, facile intersystem crossing may be induced by spin−orbit coupling (SOC), since the two degenerate π^* orbitals of $O_2^{\bullet-}$ may cause a nonzero orbital

angular momentum that can serve as a torque to flip the electron spin.[7a] Under such a condition, a pseudo-equilibrium between the singlet and triplet states will persist until a chemical reaction or escape from the effective cage removes the equilibrium. If the radical pair separates completely by the diffusion into the bulk of the solution [pathway (c)], the entire system has two totally uncoupled unpaired electrons, and therefore, the singlet pair may also be generated by the recombination of these two doublets: $^3[^2Im^{\bullet+}...S...^2O_2^{\bullet-}] \rightleftharpoons {}^2Im^{\bullet+} + {}^2O_2^{\bullet-} \rightleftharpoons {}^1[^2Im^{\bullet+}...S...^2O_2^{\bullet-}]$. Provided that there is no spin catalysis by paramagnetic additives such as transition-metal ions,[32−34] the recombination of freely diffusing radicals is the only pathway for the spin-symmetry-allowed singlet generation from the triplet pair, although this pathway is of less chemical and biological interest because of the involvement of uncontrolled radical reactions capable of carrying out oxidative damage to proteins. The direct bond-formation pathway (a) does not require any initial electron-transfer reduction of $^3O_2$, but rather the spin transition occurs somewhere along the reaction pathway leading to a cyclic peroxide.

We have examined herein the free energy changes of the electron-transfer reactions between $^3O_2$ and imidazopyrazinone derivatives with various protonation states in acetonitrile (ΔG_{ET}, eq 13), as well as those associated with the formation of a singlet 2-peroxide intermediate with gauche-out conformation induced by the attack of $^3O_2$ on the 2-position of a substrate (ΔG_{pox}, eq 14); the latter reaction involves the intersystem crossing from the triplet to singlet state.

$$Im + {}^3O_2 \rightarrow {}^2Im^{\bullet+} + {}^2O_2^{\bullet-} \qquad \Delta G_{ET} \qquad (13)$$

$$Im + {}^3O_2 \rightarrow \text{singlet 2-peroxide (gauche-out)} \qquad \Delta G_{pox} \qquad (14)$$

All possible protonation states (except for cation states) of imidazopyrazinone derivatives (**1H**), as shown in Figure S1, which includes 14 neutral, 10 monoanion, and 2 dianion states, have been considered as model substrates to be oxidized; all computed ΔG_{ET} and ΔG_{pox} values are presented in Table S1.

Figure 1A plots the ΔG_{ET} and ΔG_{pox} values against the theoretical standard redox potentials ($E_{red}°$ vs SHE) of substrates in acetonitrile. The ΔG_{ET} versus $E_{red}°$ plot gives a straight line with a slope of Faraday constant F (23.06 kcal mol^{-1} V^{-1}). The y-intercept provides a reduction potential for the $^3O_2/^2O_2^{\bullet-}$ redox couple (-0.72 V vs SHE), which agrees reasonably well with the experimental value (-0.63 V vs SHE in acetonitrile).[5] The total charge of a substrate greatly affects not only the ability

(30) (a) Noyes, R. M. *J. Chem. Phys.* **1954**, *22*, 1349. (b) Noyes, R. M. *J. Am. Chem. Soc.* **1955**, *77*, 2042. (c) Noyes, R. M. *J. Am. Chem. Soc.* **1956**, *78*, 5486. (d) Winstein, S.; Clippinger, E.; Fainberg, A. H.; Robinson, G. C. *J. Am. Chem. Soc.* **1954**, *76*, 2597. (e) Rehm, D.; Weller, A. *Ber. Bunsen-Ges. Phys. Chem.* **1969**, *73*, 834. (f) Masuhara, H.; Mataga, N. *Acc. Chem. Res.* **1981**, *14*, 312. (g) Kavarnos, G. J.; Turro, N. J. *Chem. Rev.* **1986**, *86*, 401. (h) Gould, I. R.; Young, R. H.; Moody, R. E.; Farid, S. *J. Phys. Chem.* **1991**, *95*, 2068.
(31) (a) Buchachenko, A. L.; Zhidomov, F. M. *Russ. Chem. Rev.* **1971**, *40*, 801. (b) Lawler, R. G. *Acc. Chem. Res.* **1972**, *5*, 25. (c) Kaptein, R. *Adv. Free Radical Chem.* **1975**, *5*, 381. (d) Werner, H.-J.; Staerk, H.; Weller, A. *J. Chem. Phys.* **1978**, *68*, 2419. (e) Weller, A.; Staerk, H.; Treichel, R. *Faraday Discuss. Chem. Soc.* **1984**, *78*, 271. (f) Steiner, U. E.; Ulrich, T. *Chem. Rev.* **1989**, *89*, 51.
(32) (a) Yamaguchi, K. *Chem. Phys. Lett.* **1974**, *28*, 93. (b) Yamaguchi, K. *Chem. Phys. Lett.* **1975**, *30*, 288. (c) Yamaguchi, K. *Chem. Phys. Lett.* **1975**, *34*, 434.
(33) (a) Step, E. N.; Buchachenko, A. L.; Turro, N. J. *J. Am. Chem. Soc.* **1994**, *116*, 5462. (b) Buchachenko, A. L.; Ruban, L. V.; Step, E. N.; Turro, N. J. *Chem. Phys. Lett.* **1995**, *233*, 315. (c) Buchachenko, A. L.; Berdinsky, V. L. *Chem. Rev.* **2002**, *102*, 603.
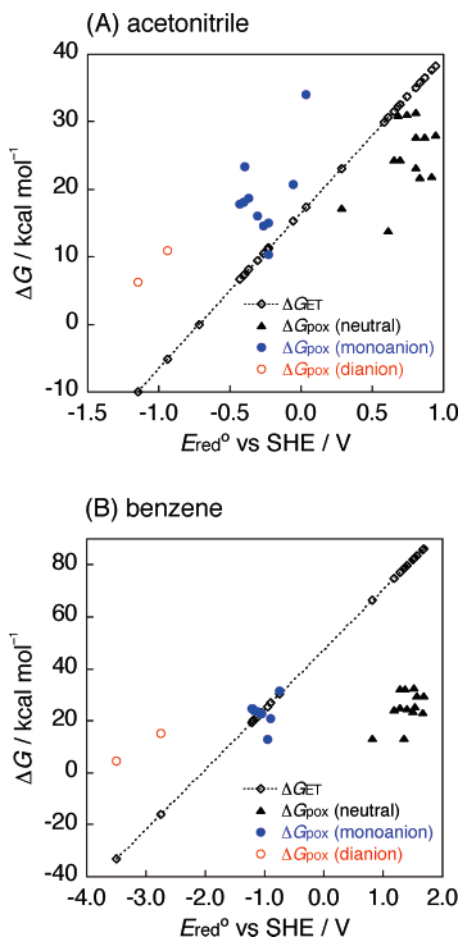(34) Minaev, B. F.; Ågren, H. *Int. J. Quantum Chem.* **1996**, *57*, 510.

Figure 1. Plots of the ΔG_{ET} and ΔG_{pox} values (eqs 13 and 14) against the theoretical standard redox potentials ($E_{red}°$ vs SHE) of imidazopyrazinone derivatives with various protonation states (Figure S1) in acetonitrile (A) and benzene (B).

to donate an electron to an extent proportional to the standard redox potential, which ranges from 0.3 to 0.9 V (versus SHE) for neutral substrates, −0.5 to 0.0 V for monoanions, and −1.2 to −0.9 V for dianions, but also its reactivity toward $^3O_2$ to give a peroxide adduct, as reflected in the relatively small ΔG_{pox} values for substrates with a negative total charge. This implies that the interaction of $^3O_2$ with an anionic substrate is important for the oxygenation reaction. It is noteworthy that there is no clear correlation between ΔG_{pox} and $E_{red}°$ among substrates with the same total charge.

Direct comparison of ΔG_{pox} with ΔG_{ET} could provide some insight to identify the mechanism indicated in Scheme 1, although the quantitative prediction cannot be discussed here for the use of free energies of reaction, instead of those of activation, the difficulty in predicting free-energy change in the condensed phase with chemical accuracy,[35] and the lack of evaluation of electronic coupling matrix elements for the electron-transfer reaction and SOC matrix elements for the intersystem crossing in acetonitrile. Given these reservations, one qualitative interpretation for the data in Figure 1A may be as follows: (i) The reaction of $^3O_2$ with a neutral substrate would

favor the direct bonding interaction over the intermolecular electron transfer because of the less endothermicity for the former. (ii) The thermoneutral condition between a bound peroxide and freely dissociated radicals for monoanionic substrates gives rise to a mechanistic borderline; given the experimental observations that the rate constant for the oxygenation reactions of **1d**$^-$ and its *para*-substituted phenyl derivatives and 3-indoyl derivative in acetonitrile increases with lowing the anodic peak potential of a substrate,[13a] the caged radical pair may be formed reversibly by complete electron transfer. (iii) The relatively large exothermicity for the electron transfer from a dianionic substrate to $^3O_2$ would enhance its rate and may result in the diffusive separation of a substrate anion radical and a superoxide anion radical.

In summary, the chemistry and activation of $^3O_2$ are directly dependent on the proton activity of a surrounding reaction field. Figure S1 summarizes computed basicities of the imidazopyrazinone substrates in dipolar aprotic solvent acetonitrile. The activity values of pK_a in acetonitrile for the generation of an anionic substrate as an electron source adequate for the reductive activation of $^3O_2$ are theoretically estimated to be ca. 20−25 except for **1fH** (ca. 11), which indicates that the presence of a base is essential in acetonitrile. This is in accordance with the experimental report that TMG, which has a moderate basicity (23.3),[36] is an appropriate base for the kinetic study of imidazopyradinones in acetonitrile.[13a] Another important factor for the activation of $^3O_2$ concerns solvent polarity, since the smaller superoxide anion tends to be better solvated by its reaction field than the larger substrate anion. The direct bond-formation pathway (a) may become complete in a less polar solvent such as benzene, even though the substrate is in a deprotonated monoanion state, since the solvation to form freely dissociated radicals becomes more endothermic and less likely to occur, as demonstrated in Figure 1B.
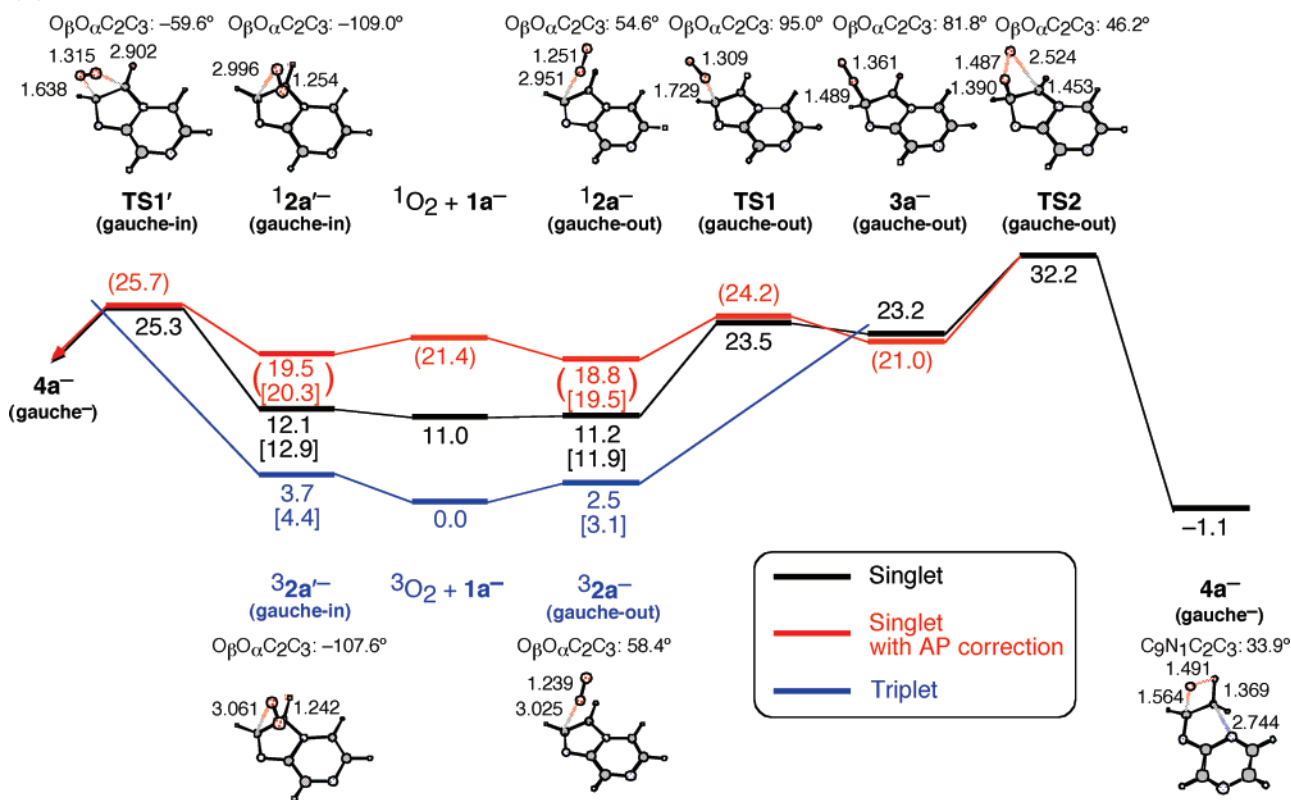
In the following subsections, we shall look more carefully into the reactions of $^3O_2$ (and also a singlet molecular oxygen, $^1O_2$) with imidazopyrazinones through three types of organization: (i) the direct pathway (a) for the monoanion state, (ii) the direct pathway (a) for the neutral state, and (iii) the stepwise pathway (c) for the dianion state, i.e., the recombination of freely dissociated anion radicals. The main discussions will be performed based on the gas-phase results, but special emphasis is placed on when the solvent effects are significant.

3.1.2. Direct Bond-Formation Pathway for Monoanion System. Let us first consider the direct bond-formation pathway (a) in Scheme 1 for the oxygenation reactions of monoanion-state (i.e., deprotonated) imidazopyrazinone derivatives **1a**−**d**$^-$. This reaction route may be important in a less polar solvent like benzene (Figure 1B). Number of calculations has clarified that the direct bonding interaction of **1a**−**d**$^-$ with either $^3O_2$ or $^1O_2$ undergoes the sequence of reactions outlined in the solid arrows in Scheme 2: (i) the formation of a triplet or singlet complex (**2**$^-$),[37] (ii) the formation of a single bond from the

(35) As mentioned in the Theoretical Background and Computational Details, there is some discrepancy between the theoretical standard redox potential and the experimental anodic peak potential of deprotonated CLA **1d**$^-$. Calibrating the theoretical redox potential may leave some room for the qualitative interpretation on the $^3O_2$ activation mechanism (Figure S4).

(36) Kolthoff, I. M.; Chantooni, M. K., Jr.; Bhowmik, S. *J. Am. Chem. Soc.* **1968**, *90*, 23.

(37) There should be a transition structure between **1**$^-$ + O$_2$ and **2**$^-$. In this study, no effort was made to characterize the transition structure, since the finding that the complexes may not be at free-energy minimum at room temperature makes the location of a transition structure on the very flat potential surface an issue of marginal importance.

Scheme 2

complex to give an open-chain 2-peroxide intermediate (3^-),[38] (iii) the oxygen–carbon bond closure of the peroxide with the simultaneous cleavage of the nitrogen–carbon bond to give a

cyclic 1,2-dioxetanone intermediate (4^-), and (iv) the decomposition of the dioxetanone to give a 2-amidopyrazine product (6^-) in the S_0, S_1, or T_1 state and a carbon dioxide (CO_2). The steps (ii) and (iv) may involve the intersystem crossing from the triplet to singlet state or vice versa. The qualitative features are found to be common among the oxygenation reactions of

(38) We have also found that imidazopyrazinones are highly subject to the attack of $^3O_2$ on the 5-position; the details of this reaction channel will be reported elsewhere in relation to the regiochemical problem.

(A) Formation of Dioxetanone

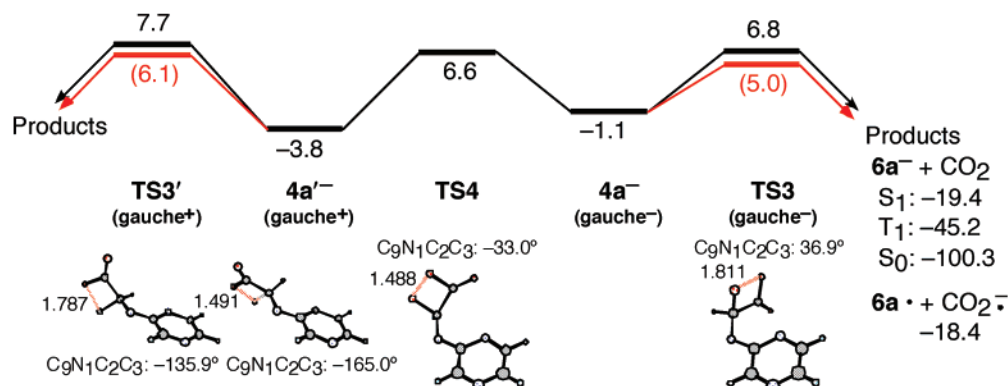## (B) Decomposition of Dioxetanone

Figure 2. Free-energy profiles in the gas phase and geometrical parameters of intermediates and transition structures in the gas phase for the reaction of $1a^-$ with O_2 at the B3LYP/6-31+G(d) level; free energies relative to reactants ($1a^- + {}^3O_2$) are given in kcal mol^{-1}; the values in parentheses are after AP correction;[17] the values in square brackets are after Boys–Bernardi counterpoise correction[40] for the basis set superposition error; bond lengths are given in angstroms; the $S_0 \rightarrow S_1$ adiabatic excitation energy of $6a^-$ (80.9 kcal mol^{-1}) was calculated by the TDDFT method using the B3LYP functional and the 6-31+G(d) basis set, based on a CIS/6-31+G(d) geometry.
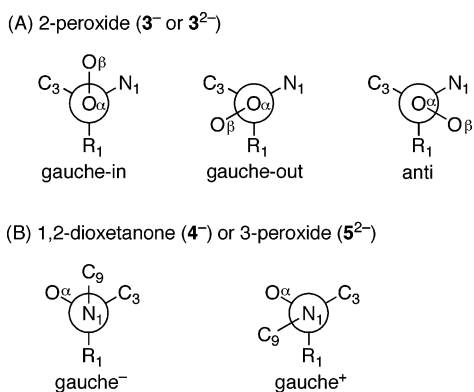
monoanionic substrates investigated by us;[39] therefore, only the results for parent imidazopyrazinone $1a^-$ are presented here in detail.

Figure 2 indicates free-energy profiles for the reaction of $1a^-$ with a molecular oxygen (O_2) in the gas phase, together with the geometrical parameters of intermediates and transition structures (TS); the corresponding energetics in the gas phase and benzene and acetonitrile solutions is summarized in Table S2 and Figure S5. The addition of ${}^3O_2$ to $1a^-$ in the gas phase

is found to occur through a weakly bound triplet complex intermediate${}^3 2a^-$ with a gauche-in or gauche-out conformation with respect to the newly forming $O_\alpha - C_2$ bond. The definition of conformations is indicated in Chart 2A by the Newman projection about the $O_\alpha - C_2$ bond looking directly down from the O_α atom toward the C_2 atom (see also Figure 2A). In the gauche-out conformation, the approaching ${}^3O_2$ molecule points in a direction away from the π-conjugated system of $1a^-$, while it sits above the imidazole ring of $1a^-$ in the gauche-in conformation (the prime symbol is used to represent the gauche-in conformation). We have also examined the pathway for the formation of a singlet 2-peroxide intermediate induced by the attack of ${}^1O_2$ on the 2-position of $1a^-$. The reaction in the gas

(39) The energetics (energies, energies including zero-point correction, enthalpies, and free energies relative to reactants) for the oxygenation reactions of neutral, monoanionic, and dianionic substrates investigated is summarized in Tables S2–S8 and Figures S5–S11.

Chart 2

(A) 2-peroxide (**3⁻** or **3²⁻**)

gauche-in gauche-out anti

(B) 1,2-dioxetanone (**4⁻**) or 3-peroxide (**5²⁻**)

gauche⁻   gauche⁺

Figure 3. Energy profiles of minimum-energy paths (MEP) for the singlet (unshaded red circles) and triplet (shaded blue circles) states against the O_α–C_2 bond length ($r_{O\alpha C2}$) and S_0 energy changes along the T_1 MEPs (red crosses) for the addition of O_2 toward **1a⁻** with the gauche-in (A) and gauche-out (B) conformations, at the B3LYP/6-31+G(d) level (top); variations of SOC matrix elements along the T_1 MEPs (bottom).

phase is found to proceed in a similar way to the triplet state, i.e., via a weakly bound singlet complex intermediate ¹**2a⁻** with a gauche-in or gauche-out conformation. The complexation enthalpies for the triplet and singlet complexes in the gas phase are calculated to be 2.7 (2.3) and 8.6 (7.8) kcal mol⁻¹ for the gauche-in (gauche-out) conformation when both the approximate spin projection (AP) correction[17] and Boys−Bernardi counterpoise correction for the basis set superposition error[40] are included (see Table S2). This large difference in the complexation enthalpy between the triplet ground and singlet excited states brings about mechanistic alternatives when large losses of entropy associated with the complexation [−25.0 (−18.5) and −25.7 (−18.7) cal mol⁻¹ K⁻¹ for the gauche-in (gauche-out) conformation at 298 K] are taken into account. The triplet complex ³**2a⁻** is not likely to be a free-energy minimum at 298 K, while a stable singlet complex ¹**2a⁻** can be formed in the gas phase with the complexation free energy of 1.1 (1.9) kcal mol⁻¹ for the gauche-in (gauche-out) conformation.[41] In what follows, we consider, as the mechanism for the reaction of ³O_2 with **1a⁻**, the direct formation of a peroxide species without the participation of a triplet complex.

The intersystem crossing from the triplet to singlet state is necessary to form two covalent bonds to give a key cyclic dioxetanone functionality. This can be accomplished when the entire system achieves a particular geometry in which the separation between the singlet and triplet states does not exceed the extent of SOC. To examine the accessibility of the crossing seam between the singlet and triplet states on multidimensional potential energy surfaces, we have determined minimum-energy paths (MEP) by the constrained geometry optimization with the O_α–C_2 bond length ($r_{O\alpha C2}$) fixed at a given value and remaining degrees of freedom relaxed. The MEP would provide a possible pathway when the system has low vibrational excess energy. The top panels in Figure 3 show the energy profiles of MEPs for the singlet (unshaded red circles) and triplet (shaded blue circles) states as a function of $r_{O\alpha C2}$ for the approach of O_2 to the 2-position of **1a⁻** with the gauche-in (A) and gauche-out (B) conformations, together with the variations in the singlet single-point energy along the triplet MEPs (red crosses). SOC
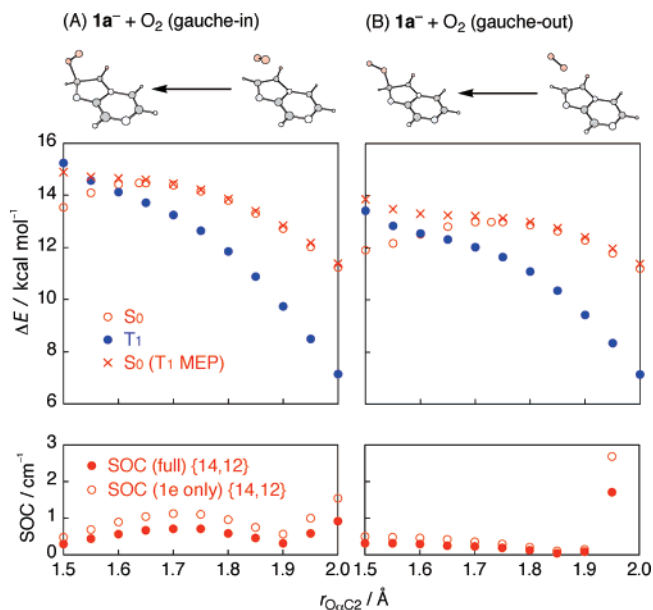
matrix elements along the triplet MEPs are indicated in the bottom panels. The interaction between ³O_2 and **1a⁻** is repulsive due to the exchange repulsion between the singly occupied $\pi*$ orbital of ³O_2 and the high-lying HOMO of anionic **1a⁻**, and the ground-state (triplet-state) energy of the system increases significantly, as ³O_2 comes close to **1a⁻**. In contrast, the formation of a O_α−C_2 covalent bond between ¹O_2 and **1a⁻** leads to marked stabilization of the system. Due to the repulsive and bonding interaction, the triplet and singlet states experience different force fields; the stable conformation for incipient triplet peroxide ($r_{O\alpha O2}$ =1.6 Å) is either gauche-in ($d_{O\beta O\alpha C2 C3}$ = −60.7°) or gauche-out (121.2°), while not only gauche-in (−55.9°) and gauche-out (85.0°) but also anti (150.2°) conformations are involved as MEP valleys for incipient singlet peroxide ($r_{O\alpha O2}$ =1.6 Å). The conformational change of the pendant O_2 in the triplet state, which would occur without a substantial barrier during the bond-formation process ($r_{O\alpha O2}$ < 1.7 Å), is, therefore, important to reach the energetically quasi-degenerate region between the singlet and triplet states, in particular for the gauche-out conformation. In this region, the system has a nonzero SOC interaction on the order of about 0.5 and 0.3 cm⁻¹ for the gauche-in and gauche-out conformations. To a greater or lesser extent, the SOC induced $T_1 \rightarrow S_0$ intersystem crossing by thermal activation is possible in this region, since the significant bonding interaction stabilizes the singlet state and destabilizes the triplet state immediately after the nonradiative transition.

The pathway which will be followed after the $T_1 \rightarrow S_0$ intersystem crossing depends entirely on the orientation of the pendant O_2 to the imidazopyrazinone substrate at the crossing seam, as shown in Figure 2A. In the gauche-in conformation, the steepest decent path leads directly to a four-membered ring dioxetanone structure **4a⁻** without passing through an open-chain 2-peroxide intermediate; i.e., the intersystem crossing occurs in concert with the ring closure with a barrier of about

(40) Boys, S. F.; Bernardi, F. *Mol. Phys.* **1970**, *19*, 553.
(41) The presence of the complexes may be questionable with the addition of solvent polarity effects, since the overall charge is less compact in the complexes than in the freely dissociated molecules. In a polar solvent such as acetonitrile, for example, the compensation effect by the destabilization due to the lower solvation of the geminate neutral−anion complex for the stabilization by the complexation brings about the net destabilization of the singlet complex ¹**2a⁻** (Table S2).

25 kcal mol^{-1} and an exothermicity of -1.1 kcal mol^{-1} in free energy. The S_0/T_1 crossing seam is regarded as a TS that connects the reactants directly to a key dioxetanone intermediate. This concerted cycloaddition process should be irreversible, since a high barrier of about 26 kcal mol^{-1} prevents effectively the ring opening of **4a**$^-$. On the other hand, a discrete 2-peroxide intermediate **3a**$^-$ exists in the gauche-out conformation; the formation of a second O–C bond requires an activation barrier of 11.2 kcal mol^{-1}.[42] The $T_1 \rightarrow S_0$ intersystem crossing is regarded as the rate-determining step in the entire oxygenation reaction of **1a**$^-$, if the reaction occurs through the direct pathway (a).

The dioxetanone formation from the 2-peroxide structure involves a simultaneous dissociation of a covalent bond between C_3 and N_4 atoms, thereby leading to flexible gauche$^-$ and gauche$^+$ conformational isomers, **4a**$^-$ and **4a′**$^-$, with respect to the N_1–C_2 single bond (the prime symbol is used to represent the gauche$^+$ conformation). The definition of the conformers is shown in Chart 2B by the Newman projection about the N_1–C_2 bond looking directly down from the N_1 atom toward the C_2 atom (see also Figure 2B). These conformers are separated by rotational barriers of 8–10 kcal mol^{-1}, while the decomposition of **4a**$^-$ and **4a′**$^-$ to afford final products amidopyrazine **6**$^-$ and CO_2 has activation barriers of 6.1 and 9.9 kcal mol^{-1}. The thermal decomposition, therefore, competes with the rotation about N_1–C_2 bond. The IRC calculations have clarified that there is no significant difference in the qualitative features of decomposition between the conformers.[43] For both **4a**$^-$ and **4a′**$^-$, the charge transfer from the electron-donor part (the amide anion group) to the electron-acceptor part (the peroxide bond) starts to come into the act, with a slight elongation of the peroxide bond to form a CT TS. Shortly after passing through the CT TS, the dissociating peroxide with CT diradical character crosses from the singlet state to a triplet state, at which point the SOC matrix elements are calculated to be 6.4 and 5.0 cm^{-1} for the gauche$^-$ and gauche$^+$ conformations. The electronic factor in intersystem crossing will be large enough at the S_0/T_1 crossing seam to allow the $S_0 \rightarrow T_1$ nonradiative transition to occur, regardless of the conformation. The dissociating peroxide that enters the triplet state then undergoes a barrierless C–C bond cleavage and decays only to the singlet ground state either nonradiatively in the vicinity of the second S_0/T_1 crossing seam (intersystem crossing) or radiatively after the formation of a triplet amidopyrazine product ^{3}**6**$^-$ (phosphorescence), since the triplet state is always lower in energy than the singlet excited state. The mechanism for the suppression of SOC in the CT diradical state of a dissociating peroxide will be discussed later.

3.1.3. Direct Bond-Formation Pathway for Neutral System. Consider next the direct bond-formation pathway (a) in Scheme 1 for the reaction of the protonated form (i.e., neutral state) of parent imidazopyrazinone **1aH** with either $^3O_2$ or $^1O_2$. It seems reasonable to suppose that the dominant protonated

forms of reactant **1a**$^-$, intermediates **3a**$^-$ and **4a**$^-$, and product **6a**$^-$ are governed by their basicities. We have assumed each protonation state for the neutral species according to the theoretical basicities in acetonitrile (Figures S1–S3); hereafter, the protonated form of **1a**$^-$, for example, is represented as **1aH$_{(X)}$**, in which X is the protonation site. The energetics for the reaction of **1aH$_{(7)}$** with O_2 is summarized in Figure S6 and Table S3. In contrast to the anion systems, the influence of solvent polarity on the energetics is rather small, unless the reaction involves an electron-transfer process. In the following, only a few aspects that are quite different from the case of monoanion systems will be briefly mentioned.

The first important aspect is that the intersystem crossing required for the formation of a cyclic peroxide structure (two-bond formation) can only occur in the ring-closure process of a bound triplet peroxide intermediate [^{3}**3aH$_{(1)}$**], irrespective of its conformation, i.e., the interaction of $^3O_2$ with **1aH$_{(7)}$** may concern the following stepwise pathway: **1aH$_{(7)}$** + $^3O_2 \rightarrow$ triplet 2-peroxide intermediate [^{3}**3aH$_{(7)}$**] $\rightarrow$ (proton transfer) $\rightarrow$ triplet 2-peroxide intermediate [^{3}**3aH$_{(1)}$**] $\rightarrow$ (intersystem crossing) $\rightarrow$ singlet dioxetanone intermediate [**4aH$_{(1)}$**]. The reason for the existence of a triplet 2-peroxide intermediate in the neutral state can be attributed to the fact that the low-lying HOMO of a neutral substrate decreases the exchange repulsion between substrate and $^3O_2$. The SOC matrix elements in the vicinity of the S_0/T_1 crossing seam are calculated to be 0.07 and 0.64 cm^{-1} for the gauche-in and gauche-out conformations, thereby suppressing intersystem crossing (via the gauche-in 2-peroxide) sufficiently. On the assumption that the oxygenation of a neutral substrate occurs exclusively via the direct pathway (a) in Scheme 1, the rate of the chemiluminescence reaction of **1aH$_{(7)}$** is predicted to be small, which is in accordance with the experimental observation that CLA [**1dH$_{(7)}$**] is inert to $^3O_2$ in aqueous buffers at a pH less than the pK_a of CLA (7.64 in aqueous solution).[12a] Another important point is that the thermolysis of neutral dioxetanone **4aH$_{(1)}$** is initiated by the homolytic O–O bond dissociation. It will be useful to keep this point in mind as we examine the extent of SOC in the thermolysis of peroxides later. Only in the final phase, the gauche-in approach of $^3O_2$ to **1aH$_{(7)}$** may give rise to several competitive reaction channels immediately after the intersystem crossing of the triplet 2-peroxide with the gauche-in conformation, ^{3}**3aH$_{(1)}$′** (Figure S6): the formation of 1,3-endoperoxide [**7aH$_{(1)}$**] with a negligible barrier and the hydroperoxidation [^{1}**3aH$_{(β)}$**] with a barrier of about 9 kcal mol^{-1}, in addition to the formation of dioxetanone **4aH$_{(1)}$** with a barrier of about 5 kcal mol^{-1}.

3.1.4. Radical Recombination Pathway for Dianion System. Let us now examine the oxygenation reactions of dianion-state imidazopyrazinones **1e**$^{2-}$ and **1f**$^{2-}$. The intermolecular electron transfer is feasible between $^3O_2$ and an electron-rich substrate with an extremely low oxidation potential. The oxygenations of **1e**$^{2-}$ and **1f**$^{2-}$ would proceed in a stepwise manner [pathway (c) in Scheme 1]: (i) the electron-transfer reduction of $^3O_2$ leading to the diffusive separation of two anion radicals, **1e**$^{•-}$ (**1f**$^{•-}$) and $^2O_2$$^{•-}$, and (ii) the homogeneous recombination of the freely dissociated anion radicals affording a bound singlet peroxide.

The primary radical separation is greatly influenced by solvent polarity. The CPCM solvation model predicts that the free

(42) The solvent polarity causes a change in the nature of the gauche-out peroxide intermediate **3a**$^-$ from diradical [dipole moment (μ) =7.7 D and diradical character (y_{HOMO}) = 12.1 % in the gas phase] to zwitterion with a large dipole moment (μ =15.9 D and y_{HOMO} = 0.0 % in acetonitrile); the same is true for the TS for the ring closure of the gauche-out peroxide intermediate. This makes the stepwise pathway via the gauche-out intermediate with zwitterionic character competitive effectively with the concerted pathway via the S_0/T_1 crossing seam in the gauche-in region with diradical character (see Table S2 and Figure S5).
(43) The energy profiles of IRC paths for **4a**$^-$ and **4a′**$^-$ are displayed in Figure S12.
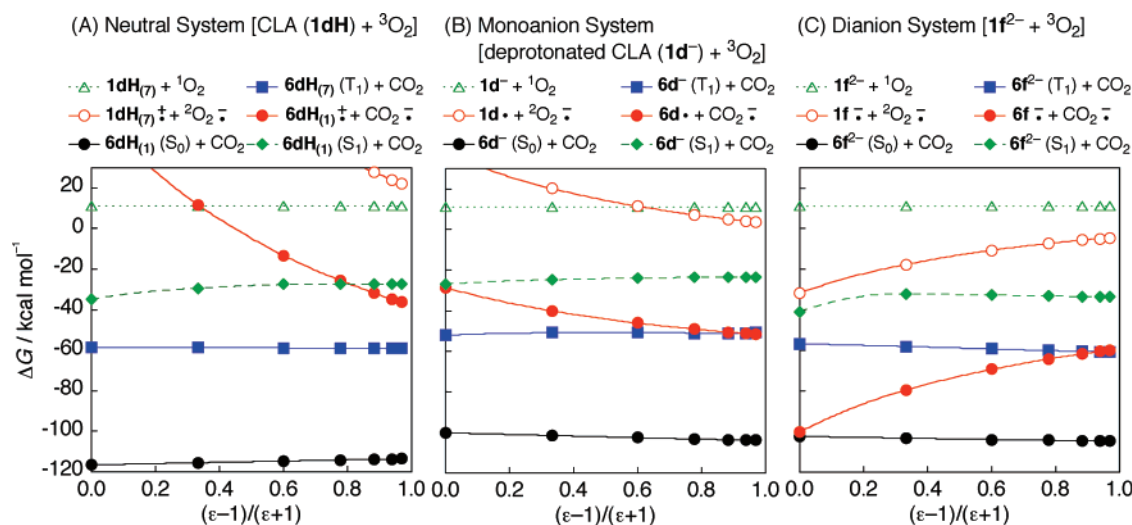
Figure 4. Solvent polarity dependence of the free energies of primary products relative to reactants (substrate + $^3O_2$) (ΔG) for the neutral [CLA (**1dH**) + $^3O_2$] (A), monoanion [deprotonated CLA (**1d$^-$**) + $^3O_2$] (B), and dianion [**1f^{2-}** + $^3O_2$] (C) systems; the reactants and primary products are considered as a freely dissociated molecule with one most stable conformation and protonation state; the free energies of products in the singlet excited state relative to reactants in a bulk solvent [$\Delta G^*_{sol}(S_1)$] were approximately evaluated according to the equation $\Delta G^*_{sol}(S_1) = \Delta G^*_{sol}(T_1) + \Delta G^*_{sol}(S_1 - T_1)$, in which $\Delta G^*_{sol}(T_1)$ is the free energy of products in the triplet state relative to reactants in a bulk solvent and $\Delta G^*_{sol}(S_1 - T_1)$ is the $T_1 \rightarrow S_1$ adiabatic excitation energy of amidopyrazine in a bulk solvent with the thermal contribution omitted, as calculated by TDDFT using the B3LYP functional and the 6-31+G(d) basis set, based on a CIS/6-31+G(d) geometry.

energies of the electron transfer from **1e^{2-}** (**1f^{2-}**) to $^3O_2$ are -63.9 (-31.7) kcal mol^{-1} in the gas phase, -33.4 (-16.2) kcal mol^{-1} in benzene, and -10.1 (-5.1) kcal mol^{-1} in acetonitrile. The relatively small thermodynamic driving force in a strongly polar solvent derives from the dielectric effect that the solvation free energy of highly charged ion **1e^{2-}** (**1f^{2-}**) is strongly negative (depending on the square of the charge) in media of a large dielectric constant.

The secondary radical recombination of the resulting radical anions, **1$^{\bullet-}$** and $^2O_2^{\bullet-}$, with singlet coupling is found to be followed by a quite different reaction sequence from that for the oxygenations of monoanionic substrates **1a$-$d$^-$**, as indicated by the dashed arrows in Scheme 2. The free-energy profiles for the reactions of **1e^{2-}** and **1f^{2-}** with O_2 are summarized in Figures S10 and S11. The interesting feature is that an open-chain 3-peroxide intermediate (**5^{2-}**) is formed directly from the radical recombination when $^2O_2^{\bullet-}$ approaches the 2-position of **1$^{\bullet-}$** with the gauche-in conformation.[44] No cyclic dioxetanone intermediate (**4^{2-}**) could be located for the oxygenations of dianionic substrates. The 3-peroxide intermediates **5e^{2-}** and **5f^{2-}** are relatively stable; barriers for the conversion into 2-peroxide or radicals are about 38$-$40 and 28$-$31 kcal mol^{-1}, and barriers for the decomposition into products are 18.1 and 7.5 kcal mol^{-1} in the gas phase. The reason for such a large stabilization of the open-chain 3-peroxide intermediate **5^{2-}**, as compared with the cyclic dioxetanone structure **4^{2-}**, can be attributed to the large resonance stabilization of the highly conjugated system, as previously pointed out by White et al. for the chemiluminescence of phenyl 9-acridinepercarboxylate anion.[45] The moment the $O_\beta-C_2$ bond is formed from **5^{2-}** to give a cyclic dioxetanone structure, the $O_\alpha-O_\beta$ bond begins to cleave without any additional barrier, and the reaction goes directly to products. The cyclic dioxetanone structure is, therefore, not a true intermediate but rather a TS in a nonsynchronous concerted mechanism.

The IRC path (the reaction pathway at 0 K) from the TS for the thermolysis of **5e^{2-}** leads gradually to closed-shell fragments,

i.e., in a direction toward amidopyrazine dianion **6e^{2-}** and CO_2; however, there is a strong possibility of complete electron transfer, since the radicals **6e$^{\bullet-}$** and $CO_2^{\bullet-}$ lie 36.1 kcal mol^{-1} below **6e^{2-}** and CO_2 in the gas phase (Table S7). The same is true of the thermolysis of **5f^{2-}**, for which **6f$^{\bullet-}$** and $CO_2^{\bullet-}$ are found only 2.1 kcal mol^{-1} above **6f^{2-}** and CO_2 (Table S8). For the same reason as mentioned above, the dielectric effect tends to decrease the thermodynamic driving force for the electron-transfer reaction. The next subsection surveys such an effect.

3.1.5. Solvent Polarity Effects on Energetics of Primary Products. In addition to the case of the reductive activation of $^3O_2$, the electron-transfer reaction has been believed to play an important role in the excitation process.[1d,46] Here, we briefly discuss the solvent polarity effects on the energetics of primary products for the oxygenation reactions of imidazopyrazinones. As representative cases, the neutral [CLA (**1dH**) + $^3O_2$], monoanion [deprotonated CLA (**1d$^-$**) + $^3O_2$], and dianion [**1f^{2-}** + $^3O_2$] systems have been investigated. All molecules examined here are considered as freely dissociated molecules. The gas-phase geometries, i.e., "planar" structures associated with the conformational alignment between the pyrazine and phenyl moieties, were used for the CPCM calculations, and the $\pi\pi^*$ singly excited singlet state was treated by the TD CPCM method,[47] based on a CI with singles (CIS)/6-31+G(d) geometry.

Figure 4 shows the solvent polarity dependence of the free energies of primary products relative to reactants (substrate + $^3O_2$) for the neutral (A), monoanion (B), and dianion (C) systems. There is a high sensitivity of freely dissociated radicals

(44) If the orientation of the approaching $^2O_2^{\bullet-}$ to **1$^{\bullet-}$** is gauche-out, the open-chain 3-peroxide intermediate can be formed in a stepwise manner via a 2-peroxide intermediate **3^{2-}**, as shown in Figures S10 and S11.

(45) White, E. H.; Roswell, D. F.; Dupont, A. C.; Wilson, A. A. *J. Am. Chem. Soc.* **1987**, *109*, 5189.

(46) The concerted or effectively concerted pathway is also a strong candidate for the excitation mechanism,[1e,4,45] especially, for the chemiluminescence of artificial systems (e.g., peroxides with an odd-patterned fluorophore). See also: (a) Catalani, L. H.; Wilson, T. *J. Am. Chem. Soc.* **1989**, *111*, 2633. (b) McCapra, F. *J. Photochem. Photobiol. A* **1990**, *51*, 21.

(47) Cossi, M.; Barone, V. *J. Chem. Phys.* **2001**, *115*, 4708.

to the solvent polarity. Under the appropriate polarity condition, the complete electron transfer may occur via a bifurcation of the potential surface from a single TS with CT diradical character.[4a] It is noteworthy that the solvent polarity can bring intramolecular charge transfer into the act even in the thermolysis of neutral peroxide, although nonpolar solvents do not have this effect.[48] In the neutral state (Figure 4A), the thermoneutral condition between the singlet excited state and the radical cation/radical anion state in a polar solvent brings about the possibility of an electron-exchange type excitation route in an "effective cage",[30a−c,33a] which may be called the CIEEL (chemically initiated electron-exchange luminescence) mechanism.[1d] In contrast, the extreme stabilization of freely dissociated radical anion species produced by the thermolysis of a dianionic peroxide may lead to the significant reduction of the cage-recombination efficiency of the radical pair (Figure 4C). In the monoanion state (Figure 4B), the neutral radical/radical anion state lies about 2−30 kcal mol^{-1} below the singlet excited state. A future molecular dynamics and/or QM/MM study will certainly be required to access to what extent the diffusive separation of radicals can be induced under experimental conditions. This subject lies beyond the scope of the present study and will not be discussed any further.

What we wish to show in the data of Figure 4 is that the lowest triplet state of the products for the neutral and monoanion systems is always lower than both the singlet excited and radical-pair states. The crossing between the singlet and triplet surfaces must occur somewhere along the reaction pathway that connects the singlet ground state of a peroxide with the singlet excited or radical-pair state of products. The intersystem crossing at the S_0/T_1 crossing seam deserves more than a passing notice. To our knowledge, this subject has been strangely neglected by chemists and biologists. The next section attempts to illustrate the regulation mechanism of the SOC of a dissociating peroxide, by which the probability of the intersystem crossing between the singlet and triplet diradical states can be affected.

3.2. Spin−Orbit Coupling in Thermal Decomposition of Peroxides. In this section, we shall analyze in detail the factors that control nonzero SOC interactions involved in the thermal decomposition of peroxides, in a similar manner to the analyses made by Salem and Rowland,[49] Michl,[50] and Danovich et al.,[51] i.e., in terms of the valence-bond description. The investigation is aimed at obtaining detailed information on how SOC can be controlled by the regulation of the protonation state of a substrate. For this purpose, we consider herein three cyclic dioxetanones, $\mathbf{4aH_{(1)}}$ (neural state), $\mathbf{4a^-}$ (monoanion state with an amide anion group), and $\mathbf{8^-}$ (monoanion state with a phenoxide anion group),[52] and an open-chain 3-peroxide $\mathbf{5e^{2-}}$ (dianion state with an amide anion and an oxy anion groups), which are regarded as simplified model substrates of chemically important protonated and deprotonated CLA, $\mathbf{4dH_{(1)}}$ and $\mathbf{4d^-}$, and biologically important luciferin-type substrates, $\mathbf{4fH_{(1)}^-}$ and $\mathbf{5f^{2-}}$ (Chart 3). The present discussions are restricted to the gas-phase results, and therefore, the conclusions deduced in this section may be most relevant to chemiluminescence in a
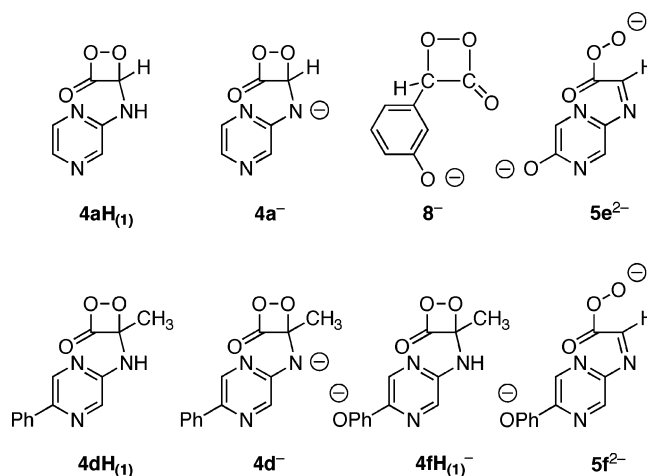
(48) See, for example, the spin density distributions of a dissociating CLA peroxide in benzene and acetonitrile solutions, as shown in Figure S17A.
(49) Salem, L.; Rowland, C. *Angew. Chem., Int. Ed. Engl.* **1972**, *11*, 92.
(50) Michl, J. *J. Am. Chem. Soc.* **1996**, *118*, 3568.
(51) Danovich, D.; Marian, C. M.; Neuheuser, T.; Peyerimhoff, S. D.; Shaik, S. *J. Phys. Chem. A* **1998**, *102*, 5923.
(52) For the mechanistic details on the thermolysis of $\mathbf{8^-}$, see ref 4a.

Chart 3

Table 1. Computed Activation Energies, O_α−O_β Bond Lengths and Diradical Characters at Transition Structures, Differences in the Mulliken Charge Density of the O_α−O_β Bond, and the Classification of Decomposition Mechanisms for the Thermolysis of Peroxides in the Gas Phase at the B3LYP/6-31+G(d) Level

peroxide	$\Delta E_{therm}^{\ddagger} + ZPC^a$	$r_{OO}^{\ddagger b}$	$y_{HOMO}^{\ddagger c}$	$\Delta\rho_{OO}^{\ddagger d}$	type^e
$\mathbf{4aH_{(1)}}$	17.1 (16.5)	2.025	16.4	−0.01	HD (FR)
$\mathbf{4a^-}$	7.9 (6.1)	1.811	1.3	−0.14	CT (AR)
$\mathbf{8^-}$	2.7 (0.9)	1.667	0.5	−0.07	CT (AR)
$\mathbf{5e^{2-}}$	17.3	1.631	0.0	0.32	CT′ (AR)
$\mathbf{4dH_{(1)}}$	17.2 (17.3)	2.001	13.3	−0.04	HD (FR)
$\mathbf{4d^-}$	8.4 (6.7)	1.818	1.5	−0.13	CT (AR)
$\mathbf{4fH_{(1)}^-}$	1.4 (−0.2)	1.638	0.2	−0.06	CT (AR)
$\mathbf{5f^{2-}}$	7.0 (6.3)	1.678	0.1	0.17	CT′ (AR)

^{a} Activation energies including zero-point correction ($\Delta E_{therm}^{\ddagger} + ZPC$) for thermolysis of peroxides are given in kcal mol^{-1}; the values in parentheses are after AP correction.[17] ^{b} O_α−O_β bond lengths at TSs ($r_{OO}^{\ddagger}$) are given in angstroms. ^{c} Diradical characters[54] at TSs ($y_{HOMO}^{\ddagger}$) are given in %. ^{d} Difference in the Mulliken charge density of the O_α−O_β bond between a peroxide intermediate and a TS. ^{e} HD represents homolytic diradical mechanism, CT charge-transfer diradical mechanism, FR forbidden-radical mechanism, and AR allowed-radical mechanism.

relatively nonpolar aprotic solvent such as benzene. We can expect, however, that the careful examination of the material can serve as a convenient introduction to understand the general trends for the regulation mechanism of SOC in CTIL.

3.2.1. Location of Transition Structures and Classification of Decomposition Mechanisms. Before proceeding to the main subject, it will be desirable to mention shortly the position of a TS on the reaction coordinate for the thermolysis of peroxides examined here and the classification of decomposition mechanisms. Table 1 summarizes activation energies including zero-point correction ($\Delta E_{therm}^{\ddagger} + ZPC$), O_α−O_β bond lengths ($r_{OO}^{\ddagger}$), and diradical characters ($y_{HOMO}^{\ddagger}$)[53] at TSs, and the differences in the Mulliken charge density of the O_α−O_β bond between a peroxide intermediate and a TS ($\Delta\rho_{OO}^{\ddagger}$) for the thermolysis of peroxides, together with their types of electronic mechanisms. Thermolysis of peroxides can be classified into two different electronic mechanisms, in terms of spin and charge distributions to a TS. One is a homolytic diradical (HD) mechanism, in which up-spin and down-spin are localized on the terminal oxygen atoms of the dissociating peroxide bond as a reflection of thermally orbital-symmetry-forbidden [2 + 2] retrocycloaddi-

(53) The diradical character is defined by the weight of the doubly excited configuration in the CASSCF theory and is formally expressed by the occupation numbers of natural orbitals in the spin-projected UDFT theory.[54]
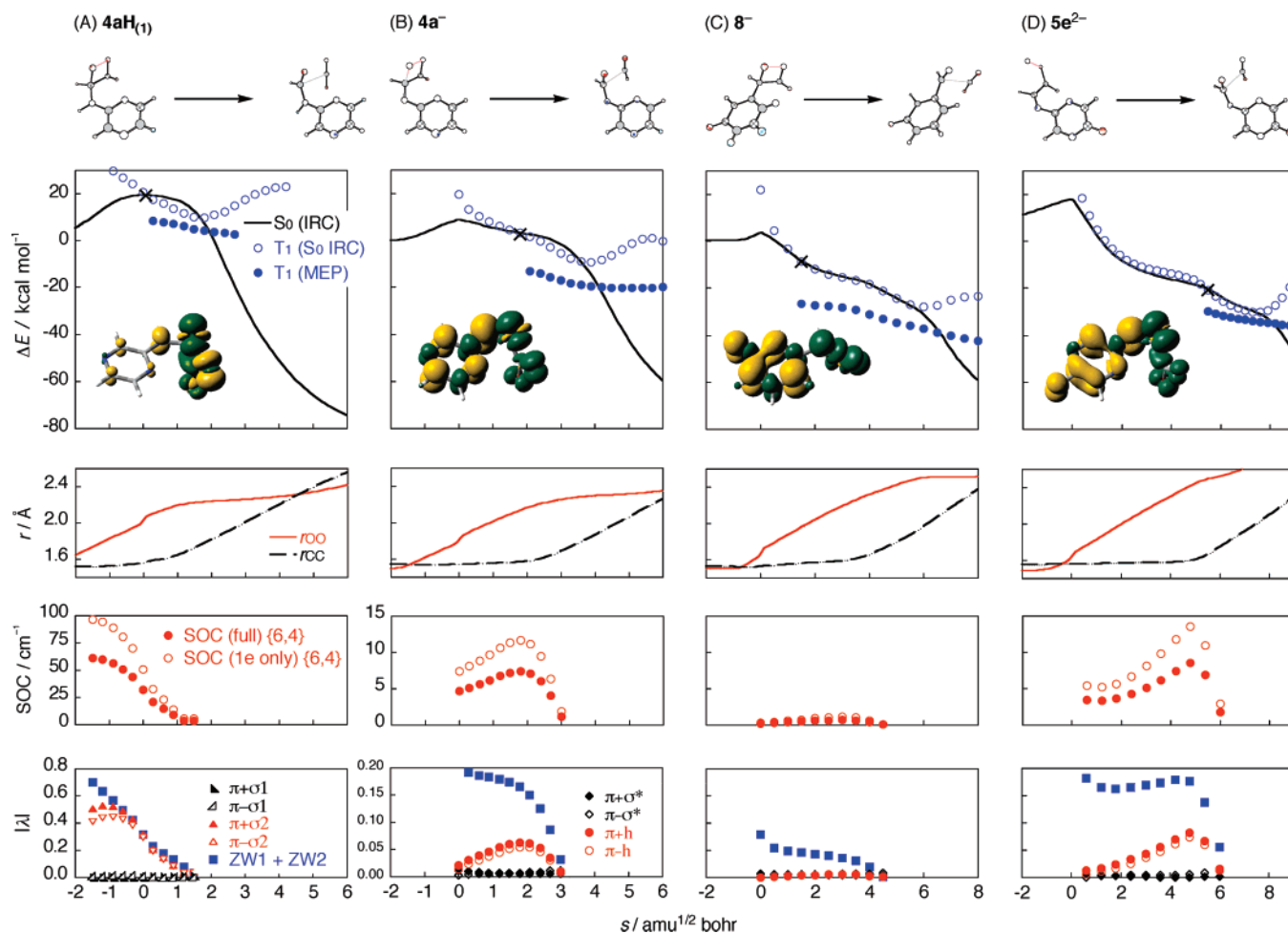
Figure 5. Energy profiles of IRC paths (solid lines) and T_1 energy changes along the IRC paths (unshaded blue circles) as a function of the reaction coordinate (s), and energy profiles of T_1 minimum-energy paths (MEP) with the C–C bond length fixed at a given value and remaining degrees of freedom relaxed (blue circles) for the thermolysis of $4aH_{(1)}$ (A), $4a^-$ (B), 8^- (C), and $5e^{2-}$ (D), at the B3LYP/6-31+G(d) level (top); singlet spin density distributions at around intersection point (crosses) as calculated by B3LYP/6-31+G(d) are inserted in top panels; variations of the C–C (r_{CC}) and O–O (r_{OO}) bond lengths along the IRC paths (second); variations of SOC matrix elements along the IRC paths (third); variations of absolute values of CI coefficients (λ) along the IRC paths (bottom).

tion. The decomposition of neutral dioxetanones $4aH_{(1)}$ and $4dH_{(1)}$ belongs to this category and exhibits high activation barriers of 16.5 and 17.3 kcal mol^{-1} with AP correction due to the violation of orbital-symmetry conservation.[55] The other is a charge-transfer (CT) diradical mechanism, in which up-spin and down-spin reside at the electron-donor part and the dissociating peroxide bond as a result of the symmetry-allowed CT orbital interaction between the HOMO of the donor and the σ^* orbital of the O–O bond acceptor. The decomposition of anionic peroxides with a substituent of sufficiently low ionization potential ($4a^-$, 8^-, $5e^{2-}$, $4d^-$, $4fH_{(1)}^-$, and $5f^{2-}$) falls into this category and provides much lower activation barriers (0–17 kcal mol^{-1}) than those of neutral dioxetanones. Further inspection of the results reveals that monoanionic dioxetanones with a phenoxide anion group (8^- and $4fH_{(1)}^-$) are located to be relatively early (small $\Delta E_{therm}^{\ddagger}$ + ZPC, $r_{OO}^{\ddagger}$, $y_{HOMO}^{\ddagger}$, and $\Delta\rho_{OO}^{\ddagger}$ values), as compared with monoanionic dioxetanones having an amide anion group ($4a^-$ and $4d^-$). As an additional

feature, the TSs for the thermolysis of open-chain 3-peroxides $5e^{2-}$ and $5f^{2-}$ with both the PhOH and N_1H groups deprotonated have a relatively high barrier, small $r_{OO}^{\ddagger}$ and $y_{HOMO}^{\ddagger}$ values, and a positive $\Delta\rho_{OO}^{\ddagger}$ value. This is because the O_β–C_2 bond ring-closure motion, which occurs in compensation for the large resonance stabilization, characterizes a vibrational component of a transition vector (Figure S13).

Starting from the TSs for the thermolysis of $4aH_{(1)}$, $4a^-$, 8^-, and $5e^{2-}$, IRC calculations have been performed to obtain reaction paths along which the extent of SOC is evaluated.[56] The top panels in Figure 5 indicate the energy profiles of the IRC paths by solid lines as a function of the reaction coordinate (s), together with the variations in the triplet single-point energy along the IRC paths and the triplet MEP energy that was obtained by the constrained geometry optimization with one frozen variable of the C–C bond length. The second panels are the variations in the O–O (r_{OO}) and C–C (r_{CC}) bond lengths along the IRC paths. The marked characteristics common to

(54) (a) Isobe, H.; Takano, Y.; Kitagawa, Y.; Kawakami, T.; Yamanaka, S.; Yamaguchi, K.; Houk, K. N. *Mol. Phys.* **2002**, *100*, 717. (b) Isobe, H.; Takano, Y.; Kitagawa, Y.; Kawakami, T.; Yamanaka, S.; Yamaguchi, K.; Houk, K. N. *J. Phys. Chem. A* **2003**, *107*, 682. (c) Isobe, H.; Yamanaka, S.; Yamaguchi, K. *Int. J. Quantum Chem.* **2003**, *95*, 532.
(55) Woodward, R. B.; Hoffmann, R. *Angew. Chem., Int. Ed. Engl.* **1969**, *8*, 781.

(56) Since the TS for the thermolysis of $5e^{2-}$ has a closed-shell configuration, the IRC path of $5e^{2-}$ was searched in the following steps: (i) first, the ordinary IRC calculation was started from the TS by using the RB3LYP method, and (ii) next, from a bifurcation point appearing on the RB3LYP IRC path ($s = 0.09917$ amu$^{1/2}$ bohr), the steepest-descent path in the mass-weighted Cartesian coordinate (which is equivalent to the IRC path) was followed by using the UB3LYP broken-symmetry solution.
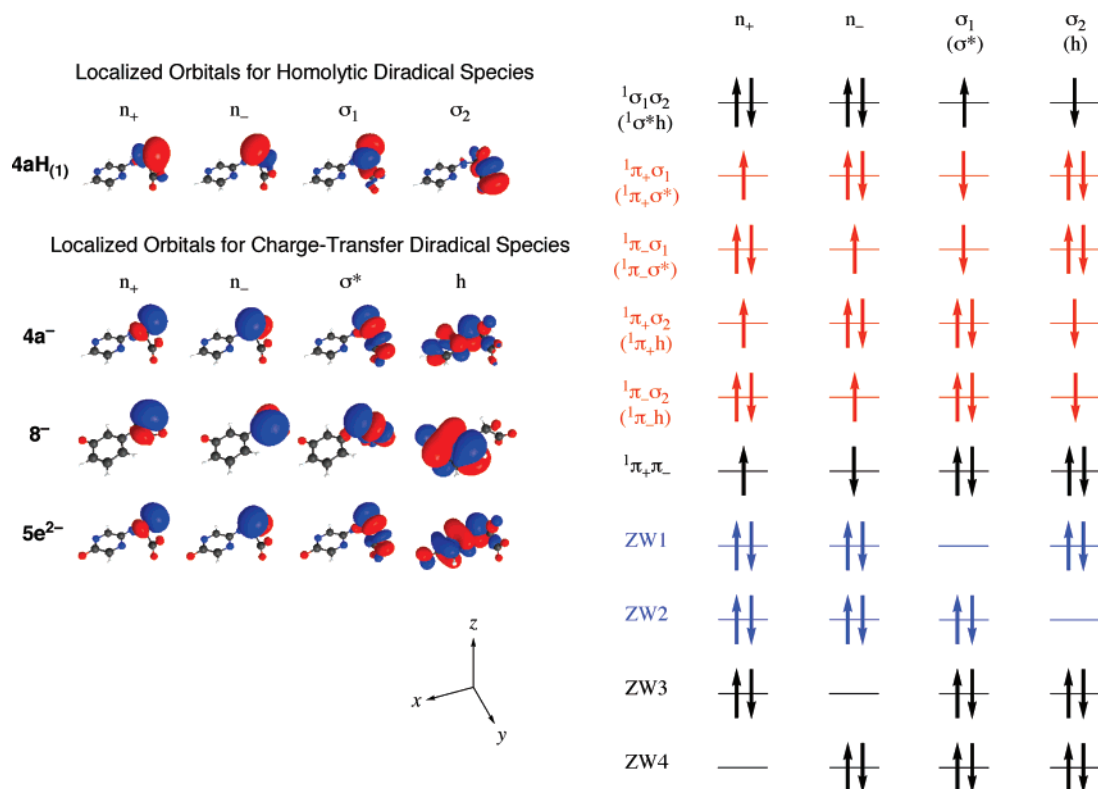
Figure 6. Boys localized orbitals in the vicinity of the S_0/T_1 crossing seam for the O−O bond breaking step of **4aH$_{(1)}$**, **4a$^-$**, **8$^-$**, and **5e^{2-}** at the ^{3}ROHF/6-31+G(d) level and the orbital diagram of singlet covalent and zwitterionic configurations.

all the IRC paths we examined are that (i) all peroxides decompose by a nonsynchronous two-stage pathway (i.e., the initial O−O bond breaking is immediately followed by the subsequent C−C bond breaking without a well-defined intermediate) and (ii) there is always a crossover of the energy of the singlet state with that of the triplet state in each step; the first S_0/T_1 crossing in the O−O bond breaking step is of great concern, since the switch from the singlet ground state to the lower-lying triplet state in this crossing region should lead to a lesser probability of the chemiexcitation to a higher-lying singlet excited state responsible for fluorescence.

3.2.2. Analysis of Spin−Orbit Coupling Using Localized Orbitals. Localized orbitals for the construction of the singlet and triplet CASCI wave functions to be used in the SOC evaluation have been generated along the IRC paths by the triplet ROHF/6-31+G(d) calculation followed by the Boys localization procedure.[27] At least four localized orbitals, as depicted in Figure 6, are found to be essential to reproduce the qualitative trends of SOC in the O−O bond breaking step; these are composed of two radical orbitals and two oxygen nonbonding orbitals. Two nonbonding orbitals, here denoted by n_+ and n_-, are common for all species, but the spatial distribution of radical orbitals reflects whether thermolysis is characterized by the homolytic or CT diradical mechanism. The σ-like orbitals localized on the oxygen atoms of the peroxide bond, which we formally call σ_1 and σ_2,[57] are important for the homolytic diradical species [**4aH$_{(1)}$**], while the CT diradical species (**4a$^-$**, **8$^-$**, and **5e^{2-}**) dictates the σ^*-like orbital of the peroxide bond

and the HOMO of the electron-donor part, which we formally call σ^* and h (Figure 6).

SOC values have been calculated along the IRC paths by using the CASCI/6-31+G(d) wave functions with the {6,4} active space, in which six electrons are distributed among the n_+, n_-, σ_1 (σ^*), and σ_2 (h) localized orbitals for homolytic (CT) diradical species. The bottom two panels in Figure 5 present the variations in the SOC value and the absolute value of the CI coefficient (λ) along the IRC paths; note that the scale on the vertical axis for **4aH$_{(1)}$** is quite different from others. The results clearly indicate that the order of SOC in the O−O bond breaking step depends entirely on the protonation state of a peroxide as follows: **4aH$_{(1)}$** $\gg$ **4a$^-$** $\simeq$ **5e^{2-}** $\gg$ **8$^-$**.[58] The SOC value of neutral **4aH$_{(1)}$** at the intersection point (ca. 30 cm^{-1}) amounts to about 60 times larger than that of **8$^-$** (ca. 0.5 cm^{-1}) and, therefore, will greatly enhance the probability of the intersystem crossing from the singlet to triplet state. The facile spin transition will contribute to the poor luminescence efficiency, since the adiabatic reaction trajectories will end up in the triplet or singlet ground state of products. The SOC values of monoanionic **4a$^-$** and dianionic **5e^{2-}** (ca. 7 and 2−8 cm^{-1}) are much smaller than that of **4aH$_{(1)}$** but still too large to suppress completely the $S_0 \rightarrow T_1$ intersystem crossing. Due to SOC values not being sufficiently large, the spin transition will behave neither adiabatically nor nonadiabatically, and the magnitude of the SOC has a great influence on the spin-state

(57) The σ_1 and σ_2 orbitals are not the "σ" orbital in a strict sense, since the σ_1 and σ_2 orbitals point in a direction unparallel to the O−O bond axis as a reflection of radical orbitals for the triplet state and have a slight delocalization tail with antibonding nature at the opposite site of the O−O bond due to the orthogonality condition among localized orbitals.

(58) To confirm whether or not the qualitative trends obtained with the {6,4} active space using Boys localized orbitals are valid, we have also evaluated SOC matrix elements by using S_0/T_1 state-averaged CASSCF{14,12}/6-31+G(d) wave functions. The SOC values at around intersection points of **4aH$_{(1)}$**, **4a$^-$**, **8$^-$**, and **5e^{2-}** are calculated to be 26.2, 6.4, 0.2, and 1.8 cm^{-1}. The {6,4} model based on localized orbitals will be adequate enough to analyze qualitatively the SOC patterns in the thermolysis of peroxides.

distributions of the products.[59] The SOC can be most effectively suppressed in the thermolysis of monoanionic **8⁻**, which is an ideal situation for chemi- and bioluminescence.

We have analyzed the origin of the nonzero SOC interaction by using the one-electron SOC operator, H_{SO1}. In the O–O bond breaking step, the triplet wave function of the homolytic diradical species **4aH(1)** using Boys localization orbitals can be satisfactorily expressed in eqs 15–17, i.e., a single covalent configuration formally described as $^3\sigma_1\sigma_2$; the weight (λ^2) of other terms are within 10^{-5} and therefore, are omitted for simplicity.

$$|^3\Psi^{(1)}\rangle = |n_+\bar{n}_+n_-\bar{n}_-\sigma_1\sigma_2\rangle \qquad (15)$$

$$|^3\Psi^{(0)}\rangle = 2^{-1/2}(|n_+\bar{n}_+n_-\bar{n}_-\bar{\sigma}_1\sigma_2\rangle + |n_+\bar{n}_+n_-\bar{n}_-\sigma_1\bar{\sigma}_2\rangle) \quad (16)$$

$$|^3\Psi^{(-1)}\rangle = |n_+\bar{n}_+n_-\bar{n}_-\bar{\sigma}_1\bar{\sigma}_2\rangle \qquad (17)$$

On the other hand, the singlet wave function is given by the superposition of six covalent configurations and four zwitterionic configurations, as shown in eq 18, in which $i = {}^1\sigma_1\sigma_2, {}^1\pi_+\sigma_1, {}^1\pi_-\sigma_1, {}^1\pi_+\sigma_2, {}^1\pi_-\sigma_2,$ and $^1\pi_+\pi_-$ (see Figure 6).

$$|^1\Psi\rangle = \sum_{i=1}^{6} \lambda_i |^1\Psi_{cov}(i)\rangle + \sum_{j=1}^{4} \lambda_{ZWj} |^1\Psi_{ZW}(j)\rangle \qquad (18)$$

The $^1\sigma_1\sigma_2$ covalent wave function is the dominant configuration with the weight of about 0.7–0.9 at around the TS region. The permissible approximation of the triplet wave function by a single configuration enables us to analyze the SOC matrix element in a simple formula. Simple algebra clarifies that nonzero elements of the k-components ($k = x$, y, and z) of the SOC matrix, $\langle^3\Psi^{(M_S)}|\hat{H}_{SO1}|^1\Psi\rangle_k$, are always proportional to the function, f_k^{HD}, as given in eq 19.[60]

$$f_k^{HD} = 2^{-1/2} \lambda_{\pi+\sigma 2}\langle n_+|\hat{h}_k|\sigma_1\rangle + 2^{-1/2} \lambda_{\pi-\sigma 2}\langle n_-|\hat{h}_k|\sigma_1\rangle$$
$$- 2^{-1/2} \lambda_{\pi+\sigma 1}\langle n_+|\hat{h}_k|\sigma_2\rangle - 2^{-1/2} \lambda_{\pi-\sigma 1}\langle n_-|\hat{h}_k|\sigma_2\rangle$$
$$+ (\lambda_{ZW1} + \lambda_{ZW2})\langle\sigma_1|\hat{h}_k|\sigma_2\rangle \qquad (19)$$

$$\left(\hat{h}_k = \frac{\alpha^2}{2}\sum_A \frac{Z_A\hat{l}_A^k}{r_A^3}\right)$$

The first four terms result from the covalent configurations, $^1\pi_+\sigma_2, {}^1\pi_-\sigma_2, {}^1\pi_+\sigma_1,$ and $^1\pi_-\sigma_1$; these terms become important when the two lone pairs of the dissociating peroxide bond, n_+ and n_-, are involved as radical orbitals in the singlet state, as shown in Figure 6. The last term stems from the zwitterionic configurations ZW1 and ZW2 which is proportional to the partial ionic character $\lambda_{ZW1} + \lambda_{ZW2}$ in the singlet state. The most important aspect of eq 19 is that the first and second terms are proportional to the one-center integrals $\langle n_\pm|\hat{h}_k|\sigma_1\rangle$ between the mutually perpendicular orbitals. Since the $\hat{l}_A^k$ operator rotates the p-type orbital by $\pm 90°$ about the axis specified by the operator subscript k, the x-component of these two terms is additive and, consequently, contributes greatly to the total SOC matrix element (y- and z-components make negligible contribution). The SOC interaction is, therefore,

(59) Schröder, D.; Shaik, S.; Schwarz, H. *Acc. Chem. Res.* **2000**, *33*, 139.
(60) For the complete expressions of the SOC matrix elements, see Table S9.

strongly enhanced when the contribution of the two covalent configurations $^1\pi_+\sigma_2$ and $^1\pi_-\sigma_2$ is significant. In fact, the bottom panel in Figure 5A shows that such a contribution is very large in the O–O bond breaking step of **4aH(1)**. This can also be recognized from the UB3LYP spin density distribution at around the first intersection point, in such a way that both the up-spin and down-spin densities emerge as σ and π at the same oxygen atom of the peroxide bond, as depicted in the top panel in Figure 5A. This is the major reason why the SOC value of the homolytic diradical species **4aH(1)** is extraordinarily large (ca. 30 cm⁻¹). The zwitterionic configurations ZW1 and ZW2 make only a minor contribution to the SOC of **4aH(1)**, since the last term in eq 19 is proportional to the two-center integral $\langle\sigma_1|\hat{h}_k|\sigma_2\rangle$ between the orbitals almost parallel to each other.

Similarly, the nonzero SOC matrix elements for the CT diradical species **4a⁻**, **5e²⁻**, and **8⁻** are directly proportional to the function f_k^{CT} as shown in eq 20;[60] we confirmed that, for all species, the weights of $^3\pi_+\sigma^*, {}^3\pi_-\sigma^*, {}^3\pi_+h,$ and $^3\pi_-h$ configurations do not exceed 10^{-6}.

$$f_k^{CT} = 2^{-1/2} \lambda_{\pi+h}\langle n_+|\hat{h}_k|\sigma^*\rangle + 2^{-1/2} \lambda_{\pi-h}\langle n_-|\hat{h}_k|\sigma^*\rangle$$
$$- 2^{-1/2} \lambda_{\pi+\sigma^*}\langle n_+|\hat{h}_k|h\rangle - 2^{-1/2} \lambda_{\pi-\sigma^*}\langle n_-|\hat{h}_k|h\rangle$$
$$+ (\lambda_{ZW1} + \lambda_{ZW2})\langle\sigma^*|\hat{h}_k|h\rangle \qquad (20)$$

In this case, first and second terms, i.e., the $^1\pi_+h$ and $^1\pi_-h$, covalent configurations, play a dominant role in determining the magnitude of SOC because of the spatial proximity of the two radical orbitals $n_\pm$ and σ^*, which is responsible for large values of the integrals, $\langle n_\pm|\hat{h}_k|\sigma^*\rangle$. The bottom panels in Figure 5 demonstrate that the contribution of this type is large for **4a⁻** and **5e²⁻** and negligible for **8⁻**, which closely correlates with the SOC values in the third panels. Thus, the great part of SOC in the CT diradical state can also be reasonably explained by the involvement of a pair of nonbonding orbitals as a radical carrier in the singlet state.

3.2.3. Relation between Spin–Orbit Coupling and Orbital Symmetry and Stability. The functions f_k^{HD} and f_k^{CT} consist of a sum of MO integrals multiplied by a configuration mixing coefficient λ. A pair of covalent terms, $^1\pi_\pm\sigma_2$ for HD and $^1\pi_\pm h$ for CT, is primarily important, since the perpendicular relation of the $n_\pm$ and σ-type (σ_1 and σ^*) orbitals in the corresponding integral part provides a significant one-center contribution to SOC. Viewed in this light, the origin of the relatively weak SOC induced by intramolecular CT, as compared with that by homolytic O–O dissociation, can be ascribed to the following two points. The first is that the magnitude of the integrals $\langle n_\pm|\hat{h}_k|\sigma^*\rangle$ for CT is smaller than that of the integrals $\langle n_\pm|\hat{h}_k|\sigma_1\rangle$ for HD due to the delocalization of the σ^* orbital (Figure 6), which is responsible for a smaller one-center contribution. The second and even more important factor relates to the weights of covalent CI coefficients, i.e., the contribution of a pair of nonbonding orbitals as a radical orbital in the singlet state; they differ by a factor of about $10-100$ between the homolytic and CT diradicals. The key $^1\pi_\pm\sigma_2$ and $^1\pi_\pm h$ covalent configurations for HD and CT can be generated from the dominant configuration, $^1\sigma_1\sigma_2$ and $^1\sigma^*h$, by the transition of an electron from the $n_\pm$ orbitals to the σ-type (σ_1 and σ^*) orbital, as can been seen from the orbital diagram in Figure 6. The most essential factor to induce such an electronic fluctuation is to introduce the
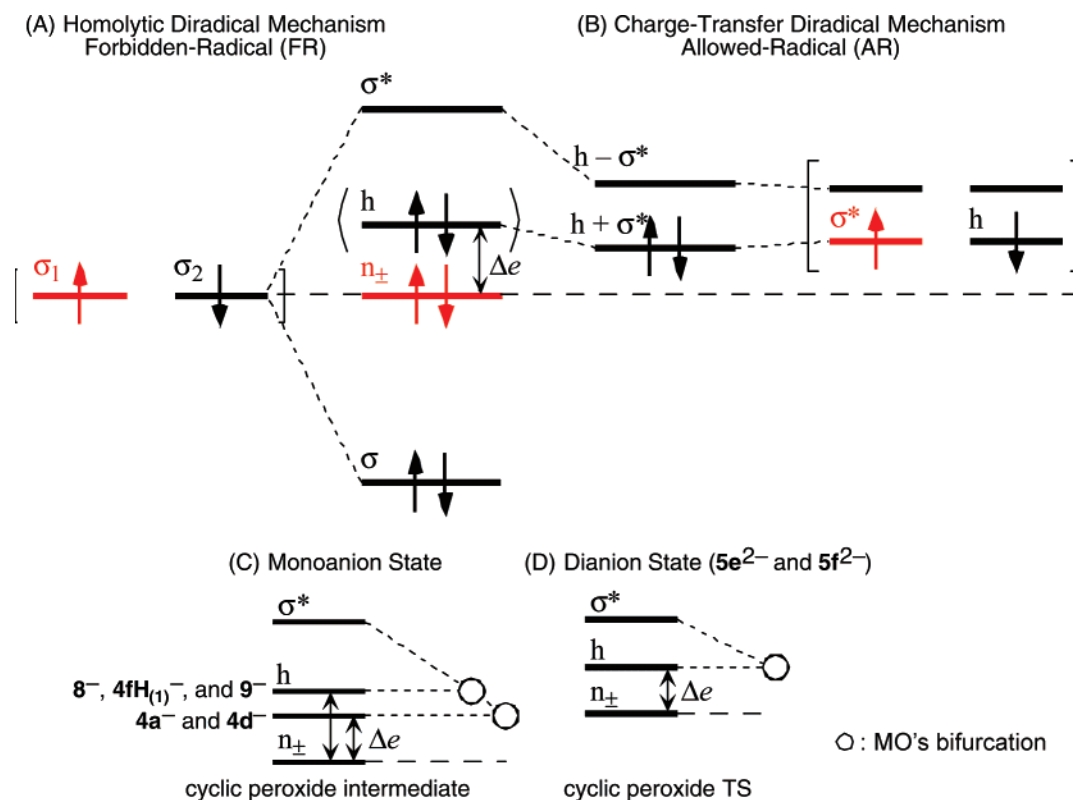
Figure 7. Schematic orbital-interaction diagrams for the thermolysis of peroxides in homolytic diradical mechanism (A) and charge-transfer diradical mechanism (B) in monoanion state (C) and dianion state (D). The total number and nature of available radical orbitals[65] created in the decomposition reaction of a peroxide has a dramatic effect on the magnitude of SOC: A and B explain how the switch of the topicity label [$(\sigma_1, n_+, n_-)\sigma_2$ tetratopic (forbidden-radical) $\rightarrow$ (σ^*, n_+, n_-)h tetratopic (allowed-radical)] affects the generation of a magnetic torque by a dynamical electronic fluctuation to cause spin flip; C and D explain how the change in the topicity number [(σ^*, n_+, n_-)h tetratopic (small Δe) $\rightarrow$ σ^*, h bitopic (large Δe)] affects the generation of a magnetic torque.

orbital-symmetry-forbidden character into the singlet wave function, as is done in the homolytic diradical mechanism. In the broken-symmetry picture, the quasi-degeneracy of the bonding and antibonding σ orbitals for a sufficiently O−O elongated structure provokes strong triplet instability, and therefore, they should be reorganized into the different orbitals for different spin (DODS) type molecular orbitals ($\psi^\pm$),[17a,54,61] which are given by a strong mixing of the σ and σ^* orbitals, as shown in eq 21, in which ω is the orbital mixing coefficient ($0° < \omega \leq 45°$).[4d,62]

$$\psi^\pm = \cos\omega\sigma \pm \sin\omega\sigma^* \qquad (21)$$

The spin-polarized orbitals ($\psi^\pm$), which correspond to the σ_1 and σ_2 orbitals in Figure 6, are sufficiently localized on the oxygen atoms and are effectively chemically equivalent to the $n_\pm$ orbitals, leading to a small orbital-energy separation between the $n_\pm$ and σ_1 orbitals, as shown in Figure 7. This is the reason for a very large fluctuation associated with the motion of a localized electron, $n_\pm \leftrightarrow \sigma_1$ (i.e., strong resonance hybrid of the $^1\sigma_1\sigma_2$ and key $^1\pi_\pm\sigma_2$ configurations) in the homolytic diradical mechanism. Such a dynamical electronic fluctuation between the singlet and triplet wave functions creates an instantaneous orbital angular momentum that can flip the electron spin such that the total angular momentum of the system is conserved. On the other hand, the presence of the high-lying

HOMO of donor (h) in the CT diradical mechanism causes a change in the orbital symmetry−stability relation from forbidden-radical (FR) to allowed-radical (AR) in our terminology,[54,62] as shown in Figure 7. In this case, only weak CT orbital interaction caused by a slight O−O elongation is sufficient enough to initiate an irreversible O−O bond breaking, since the decrease in the HOMO−LUMO gap readily induces a CT excitation (occupation of the LUMO), which results in a further O−O breaking and a stronger CT interaction. The resulting bonding (h + σ^*) and antibonding (h − σ^*) orbitals bifurcate into DODS orbitals; the bonding DODSs are rather similar to the h and σ^* orbitals.[63] Mechanistically significant, these spin-polarized orbitals are not chemically equivalent to the $n_\pm$ orbitals. The appreciable energy separation between the $n_\pm$ and σ^* orbitals is responsible for the suppression of a fluctuation associated with the motion of a localized electron, $n_\pm \leftrightarrow \sigma^*$ (small resonance contribution of the key $^1\pi_\pm$h configurations) and therefore weak (but still nonzero) SOC, as compared with the homolytic diradical mechanism.

3.2.4. Favorable Conditions for Suppression of Spin− Orbit Coupling. The extent of SOC in the CT diradical mechanism is greatly influenced by the protonation-state identity and is reasonably correlated with the position of a CT TS on the reaction coordinate, as schematically represented in Figure 8. The CT TS varies its position according to the electron-donor and electron-acceptor capability.[4] The relatively late CT TS for the thermolysis of monoanionic dioxetanone **4a⁻** with the N_1H

(61) Soda, T.; Kitagawa, Y.; Onishi, T.; Takano, Y.; Shigeta, Y.; Nagao, H.; Yoshioka, Y.; Yamaguchi, K. *Chem. Phys. Lett.* **2000**, *319*, 223.
(62) Yamaguchi, K.; Fueno, T.; Fukutome, H. *Chem. Phys. Lett.* **1973**, *22*, 466.
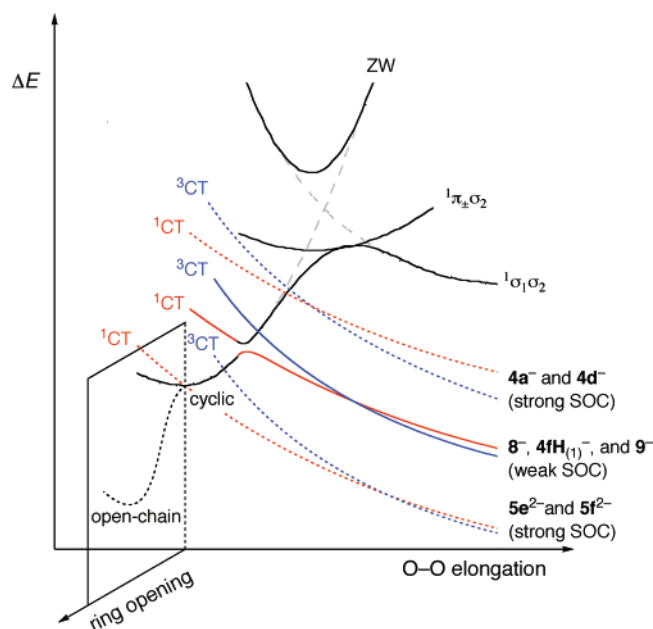
(63) See, for example, Figure 2B in ref 4a.

Figure 8. Schematic presentation of the relation between the position of a CT TS and the extent of SOC for the thermolysis of peroxides. The ground-state adiabatic surface for neutral peroxides leads smoothly to a homolytic diradical state, in which the $^1\sigma_1\sigma_2$ covalent configuration is dominant, as a consequence of the strongly avoided crossing between the ground and doubly excited molecular orbital configurations (black solid lines). When an electron-donating substituent is present (e.g., monoanionic peroxides 8^-, $4fH_{(1)}^-$, and 9^-), the adiabatic surface can then lead to a CT diradical state (red lines), in which the $^1\sigma^*h$ covalent configuration is dominant. The avoided crossing is reflected by a potential barrier on the ground surface via a short region that can be characterized by an endothermic intramolecular CT TS (the mixing of the ground and $^1\sigma^*h$ configurations, see ref 4), and its barrier height depends on the electron-donating capability of the donor part (red lines). In a special case in which the ionization potential of the donor part is extremely low (dianionic peroxides $5e^{2-}$ and $5f^{2-}$), an open-chain 3-peroxide structure becomes stabilized (a black dashed line), and consequently, an additional barrier is required to form a cyclic dioxetanone structure (TS). The extent of SOC between the singlet and triplet CT diradical states is found to be correlated with the position of a CT TS on the reaction coordinate.

group deprotonated results in relatively strong SOC at the intersection point between the ^{1}CT and ^{3}CT diradical states. The CT TS becomes extremely early under the influence of the phenoxide anion group as an electron donor, as does in the thermolysis of monoanionic dioxetanone 8^-, for which SOC is negligible. An extremely low ionization potential of the electron donor part of dianionic peroxide $5e^{2-}$ is apparently expected to bring about barrierless decomposition; however as it turned out, the O_β–C_2 bond formation from the open-chain peroxide structure requires a high activation barrier for overcoming the loss of large resonance stabilization, and SOC is enhanced again. An important conclusion is that there exists an optimal protonation state for the suppression of SOC in the CT-induced decomposition of peroxides: the earlier the CT TS, depending on the protonation state, the weaker the SOC.

We now explain the cause of the dependence of SOC on the protonation state of a CT diradical species by using the broken-symmetry approach, as shown in Figure 7. First, we thought that the conformational alignment between the two lone-pair orbitals of the N_1 nitrogen and the σ^* orbital of the peroxide bond is essential; however, the absence of an appreciable difference between gauche$^+$ and gauche$^-$ conformers $4a^-$ and $4a'^-$ (Figure S12) rules out to some extent this possibility, as

far as the parent system is concerned. Based on the careful examination of the Kohn–Sham orbital energies of the HOMO of donor (h) and the σ^* and nonbonding (n) orbitals of the peroxide bond for cyclic peroxide intermediates in the monoanion state and cyclic peroxide TSs in the dianion state (see Table S10 and Figure S14), we consider the energy level of the HOMO relative to that of the nonbonding orbital (Δe) as a decisive factor controlling SOC. According to Koopmans' theorem, the ionization potential is reasonably well approximated by minus the orbital energy of the MO from which an electron is removed. A small difference in the ionization potential of an electron-donor part [2.23 eV for 2-amidopyrazine anion and 2.14 eV for phenoxide anion at the B3LYP/6-31+G(d) level] is manifest in a large difference in the Δe value of a dioxetanone intermediate in the monoanion state (0.065 au for $4a^-$ and 0.142 au for 8^-); the h orbital lies much higher relative to the n orbital with the deprotonation of the phenolic OH group than with the deprotonation of the N_1H group, as illustrated in Figure 7C. The larger Δe value for 8^- leads to an earlier CT TS and weaker SOC, while a later CT TS and stronger SOC stem from the smaller Δe value for $4a^-$. The deprotonation of both the phenolic OH and N_1H groups causes a marked rise in the energy levels of not only the h orbital but also the n orbital due to strong interelectronic repulsion that pushes up all occupied orbitals (Figure 7D). The contracted n orbital receives a more drastic response to the interelectronic repulsion than the diffuse h orbital. The net effects result in a small Δe value and strong SOC for $5e^{2-}$, despite its extremely low ionization potential of the donor [−3.16 eV for 5-oxy-2-amidopyrazine dianion].

One may pose a question about the validity of the simplification of the structures of CLA and luciferin-type substrates, e.g., the omission of the amino and pyrazine bridges for 8^-. To verify whether the arguments, deduced for the simplified model substrates, $4aH_{(1)}$, $4a^-$, 8^-, and $5e^{2-}$, are relevant to more realistic models, we have also investigated the thermolysis of $4dH_{(1)}$, $4d^-$, $4fH_{(1)}^-$, and $5f^{2-}$ in the same manner. The results, as demonstrated in Figures S15 and S16, are found to reproduce satisfactorily the major trends observed for the simplified models shown in Figures 5 and 6. From these consistent results, several important requirements for the suppression of SOC in the gas phase become very clear:[64] (i) the deprotonation to generate an anionic form of an electron donor with a low ionization potential is indispensable, (ii) the phenoxide anion group is by far a better electron donor than the amide anion group, and (iii) the phenoxide anion group should act as a sole electron donor; i.e., the monoanion state is preferred over the dianion state.

There is further evidence to suggest the importance of the deprotonation of the phenolic OH group in CTIL. We have also examined the thermolysis of dioxetanone intermediates of firefly luciferin, $9H$ (protonated form) and 9^- (deprotonated form) (Chart 4), which have a sulfur-containing heteroring as an activator and a fluorophore, a quite different structure from the imidazopyrazinone skeleton, but have a common phenolic OH group as a potent electron-donor group and a dioxetanone functionality as an energy source. As reported previously,[4a] neutral $9H$ decomposes by forbidden-radical (FR) homolytic

---

(64) Of course, the optimal protonation state for the suppression of SOC may be changed according to a surrounding reaction field such as environmental polarity, specific (localized) short-range interactions, etc. that can shift the occupying high-energy orbitals of a substrate. The requirements (i)−(iii), therefore, may be most relevant to chemiluminescence in a relatively nonpolar aprotic solvent.

Chart 4

9H, R = OH

9⁻, R = O ⊖
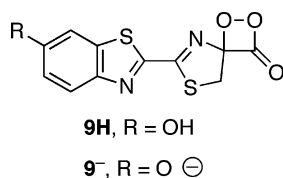
O−O dissociation with a high activation barrier of 16.3 kcal mol^{-1} with both AP and ZPC included, while allowed-radical (AR) intramolecular CT comes into the act in the thermolysis of anionic **9⁻** via an early TS with a low activation barrier of 1.8 kcal mol^{-1}. It is not surprising that the homolytic diradical mechanism for **9H** leads to strong SOC (ca. 25 cm^{-1}) in the vicinity of the S_0/T_1 crossing seam, while weak SOC (ca. 0.2 cm^{-1}) stems from the CT diradical mechanism for **9⁻**, as shown in Figures S15 and S16.

The favorable conditions for the suppression of SOC (i)−(iii), as mentioned above, are to minimize the CI coefficients of the residual covalent configurations (especially, $^1\pi_\pm$h configurations) by the regulation of the protonation state of the electron-donor part. Another factor that determines the extent of SOC will definitely be the electron-acceptor part, i.e., whether the energy source concerns the dioxetanone or dioxetane functionality. This is a very interesting issue in relation to the regiochemical problem, since the dioxetanone functionality can only be generated by the attack of O_2 on the 2-position of an imidazopyrazinone substrate. The detailed investigation of regioselectivity is now in progress.

Upon the appropriate regulation of the protonation state of a substrate, the CT diradical state of a dissociating peroxide can be reasonably described in the framework of two electrons in two orbitals, and the function f_k^{CT} becomes proportional to the zwitterionic character ($\lambda_{ZW1} + \lambda_{ZW2}$) in the singlet CT diradical state, as shown in eq 22.

$$f_k^{CT} \cong (\lambda_{ZW1} + \lambda_{ZW2})\langle\sigma^*|\hat{h}_k|\text{h}\rangle \qquad (22)$$

The complete suppression of SOC, therefore, can be accomplished when the system has pure diradical character. The adjustment of a reaction field with varying degrees of polarity may be helpful in approaching such an extreme condition. Apart from the vibronic degeneracy between the singlet and triplet states, however, there are sufficient reasons for accepting that the zwitterionic character pales in significance in the intersystem crossing. One is that SOC will not be so strong even when the system has a certain degree of zwitterionic character, since two radical orbitals σ^* and h, which are far away in space to each other, make a small contribution to the integral $\langle\sigma^*|\hat{h}_k|\text{h}\rangle$ (see, for example, localized orbitals for **4fH(1)⁻** and **9⁻** in Figure S15). In fact, the SOC value for the thermolysis of **4fH(1)⁻** and **9⁻** should not exceed ca. 1.5 cm^{-1} in the framework of two electrons in two orbitals even when the zwitterionic character of a dissociating peroxide increases to 0.3. Such weak interaction will not significantly influence the rate of intersystem crossing. Another reason is that the absence of the intermediary formation of a CT diradical having an appreciable lifetime, as shown in the top panels of Figure 5 and Figure S16, will no longer cause a Boltzmann distribution between the singlet and triplet states. It will be possible to produce an emitter so that nonequilibrium population of the higher-lying singlet state occurs. This is in

Chart 5

10H   **11H**
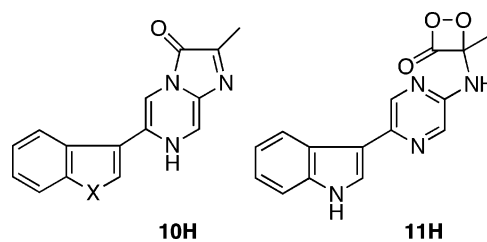
sharp contrast with the situation for the thermal activation for the $^3O_2$ reaction.

We feel that the adjustment of the reaction field is rather important for the branching in the reaction route. In particular, the electron-transfer reaction illustrates the interplay between covalent and zwitterionic surfaces.[4a,65] The radical dissociation may occur under the appropriate polarity condition via a bifurcation of the potential surface from a transient CT diradical species. The crossing between the singlet and triplet surfaces should occur before the bifurcation into adiabatic back CT (zwitterionic surface)[66] and complete electron transfer (covalent surface), which is assumed to occur during the C−C bond breaking step.[4a] SOC at the S_0/T_1 crossing seam in the O−O bond breaking step, therefore, has a great influence on the spin-multiplicity distribution and the excitation yield in product formation, regardless of the reaction route, and the suppression of the SOC of a dissociating peroxide will constitute a necessary condition for the high efficiency of chemi- and bioluminescence.[67] We feel that the enzyme should regulate the protonation state of a peroxidized substrate to minimize SOC such that vast amounts of energy released on the oxidation of the substrate do not leak out to a nonluminescent triplet state. In this line of thought, further work is now in progress.

3.2.5. Comparison with Experiment. Recently, Takahashi et al.[13c] have reported that the quantum yield for the chemiluminescence of the neutral derivatives of 6-(3-indoyl)-2-methylimidazopyrazinone (**10H**), as shown in Chart 5, the model substrates of *Cypridina* luciferin **1hH**, is affected in diglyme/acetate buffer by the electron-donating ability of a substituent (X = NH, NCH$_3$, S, or O). Interestingly, our preliminary calculations show that neutral dioxetanone with a 3-indoyl group (**11H**), as shown in Chart 5, decomposes via a relatively late TS through the CT diradical mechanism even in a less polar solvent like benzene (see Figure S17B). On the assumption that a neutral dissociating peroxide with CT diradical character behaves neither adiabatically nor nonadiabatically at the S_0/T_1 crossing seam and that the diffusive separation of radicals by electron transfer is effectively suppressed, our theoretical considerations reported in this paper appear to be consistent with their experimental observations: the greater the electron-donating ability of a substituent, the higher the chemiluminescence quantum yield. Although the assignment of the origin of

(65) (a) Dauben, W. G.; Salem, L.; Turro, N. J. *Acc. Chem. Res.* **1975**, *8*, 41. (b) Salem, L. *Science* **1976**, *191*, 822.

(66) The nonadiabatic back CT for the direct generation of the singlet excited state requires a S_0/S_1 conical intersection or a weakly avoided crossing along the reaction coordinate.[4a] At the present stage, we have no definite information on the existence of them in the thermolysis of imidazopyrazinone peroxides.

(67) If the diffusive separation of radicals is feasible, as it would be in the thermolysis of dianionic peroxides **5**$^{2-}$ (Figure 4C), the suppression of the SOC of a dissociating peroxide becomes a trivial problem, in the sense that the spin coupling between free radicals distributed in the bulk solvent results in the scrambling of the two spin states of products.

the high efficiency of complex chemiluminescence reaction to one factor is crude and should be done with appropriate skepticism, we feel that their experimental data on neutral dioxetanones reflect, to a certain extent, the violation of spin-symmetry conservation along the reaction pathway.

4. Conclusions

The present study surveys the spin transition in the reactions of imidazopyrazinone derivatives (**1H**) with $^3O_2$. The generation of an anionic substrate as an adequate electron source is important for the reductive activation of $^3O_2$. Such substrate activation for the $^3O_2$ reaction is affected by the proton activity and solvent polarity of a surrounding reaction field. An important factor that controls SOC in the thermolysis of a resulting peroxide adduct is the protonation state of the substrate. The optimal suppression of the SOC of a dissociating peroxide is achieved when the CT TS occurs early in the reaction, which is the case when an electron-donating (deprotonated OH) substituent is present. The first and foremost important point for the regulation of SOC in the CT diradical state is that the elimination of residual covalent configurations from the singlet wave function removes one-center contribution to SOC. The minor point is that the spatial separation between the electron-donor part and the electron-acceptor part (the peroxide bond) reduces two-center contribution to SOC via zwitterionic configurations. On these grounds, we arrive at the conclusion that, from the point of view of the spin transition from the triplet state of reactants to an overall singlet state of primary products, the best protonation state for the charge-transfer-induced luminescence (CTIL) of imidazopyrazinone derivatives in the gas phase is the monoanion state with the phenolic OH group deprotonated.

Supporting Information Available: The following data are provided: complete ref 19; basicities of reactants, intermediates, and products; theoretical standard redox potentials of substrates; modified version of Figure 1 using calibrated redox potentials; energetics for the oxygenations of imidazopyrazinones; energy profiles of IRC paths for the thermolysis of **4a**$^-$; imaginary vibration modes at TSs for the thermolysis of **5e**$^{2-}$ and **5f**$^{2-}$; SOC matrix elements, Kohn–Sham orbital energies, Boys localized orbitals, IRC analyses, and spin density distributions for the thermolysis of peroxides; and Cartesian coordinates and absolute energies of optimized structures reported. This material is available free of charge via the Internet at http://pubs.acs.org.

JA073834R